bioRxiv preprint doi: https://doi.org/10.1101/2023.06.15.545082; this version posted June 15, 2023. The copyright holder for this preprint (which was not certified by peer review) is the author/funder, who has granted bioRxiv a license to display the preprint in perpetuity. It is made available under aCC-BY-NC-ND 4.0 International license.

Transgene directed induction of a stem cell-derived human embryo model

Bailey AT Weatherbee[1]*, Carlos W Gantner[1]*, Riza M Daza[2], Nobuhiko Hamazaki[2], Lisa K. Iwamoto-Stohl[1], Jay Shendure[2,3,4,5] & Magdalena Zernicka-Goetz[1,5,6†].

[1]Department of Physiology, Development and Neuroscience, University of Cambridge, Cambridge, UK.

[2]Department of Genome Sciences, University of Washington School of Medicine, Seattle, WA, USA.

[3]Brotman Baty Institute for Precision Medicine, Seattle, WA, USA.

[4]Howard Hughes Medical Institute, Seattle, WA, USA.

[5]Allen Discovery Center for Cell Lineage Tracing, USA.

[6]Division of Biology and Biological Engineering, California Institute of Technology, Pasadena, CA, USA.

*Equal contribution.

[†]Correspondence and requests for materials should be addressed to M.Z-G.

Abstract

The human embryo undergoes morphogenetic transformations following implantation into the uterus, yet our knowledge of this crucial stage is limited by the inability to observe the embryo *in vivo*. Stem cell-derived models of the embryo are important tools to interrogate developmental events and tissue-tissue crosstalk during these stages[1]. Here, we establish a human post-implantation embryo model comprised of embryonic and extraembryonic tissues. We combine two types of extraembryonic-like cells generated by transcription factor overexpression with wildtype embryonic stem cells and promote their self-organization into structures that mimic aspects of the post-implantation human embryo. These self-organized aggregates contain a pluripotent epiblast-like domain surrounded by hypoblast- and trophoblast-like tissues. We demonstrate that these inducible human embryoids robustly generate several cell types, including amnion, extraembryonic mesenchyme, and primordial germ cell-like cells in response to BMP signaling. This model also allowed us to identify an inhibitory role for SOX17 in the specification of anterior hypoblast-like cells[2]. Modulation of the subpopulations in the hypoblast-like compartment demonstrated that extraembryonic-like cells impact epiblast-like domain differentiation, highlighting functional tissue-tissue crosstalk. In conclusion, we present a modular, tractable, integrated[3] model of the human embryo that will allow us to probe key questions of human post-implantation development, a critical window when significant numbers of pregnancies fail.

Introduction

Human reproduction is remarkably inefficient, with an estimated 60% of pregnancies failing during the first two weeks following fertilization[4,5]. Since the advent of *in vitro* fertilization, human embryos have been studied throughout the first week of development[1,6]. However, the second week, which includes implantation into the uterus and preparation for gastrulation, remains a 'black box[5]'. The

bioRxiv preprint doi: https://doi.org/10.1101/2023.06.15.545082; this version posted June 15, 2023. The copyright holder for this preprint (which was not certified by peer review) is the author/funder, who has granted bioRxiv a license to display the preprint in perpetuity. It is made available under aCC-BY-NC-ND 4.0 International license.

human blastocyst at 5-6 days post-fertilization consists of the outermost trophectoderm, precursor of the placenta, and inner cell mass, which gives rise to both the embryonic epiblast and the yolk sac precursor, the hypoblast. Between 7-8 days post-fertilization the blastocyst implants into the endometrium and the epiblast polarizes and transitions from the naïve state of pluripotency to the primed state[1]. A central amniotic cavity forms within the epiblast, separating the dorsal amniotic epithelium and the ventral epiblast, which maintains pluripotency and gives rise to the embryo proper[1]. The trophectoderm develops into several trophoblast subtypes following implantation[7] and the hypoblast forms the primary, and then secondary, yolk sac. A subset of cells in the hypoblast maintains expression of NODAL, BMP and WNT inhibitors, safeguarding the future anterior epiblast from posteriorizing signals during primitive streak formation, marked by upregulation of BRY/TBXT[2]. An additional extraembryonic tissue, the extraembryonic mesenchyme, is located between the inner cell mass-derived tissues and the trophoblast, however, the origin of these cells remains unclear[8].

Recent work in mouse embryos established conditions amenable to human embryo *in vitro* culture through implantation, opening this developmental black box for the first time[9-12]. We and other groups have used this system to characterize major developmental events, including formation of the anterior hypoblast domain, specification of trophoblast subtypes and transitions in epiblast pluripotency state[2,7,13-15]. However, mechanistic work in the human embryo remains challenging. Thus, stem cell-derived models of the human embryo will serve as an important and complementary tool to understanding this crucial period of our development. Several groups have reported the generation of blastocyst-like structures derived from human embryonic stem cells (hESCs)[16-20]. These ‘blastoids’ resemble the pre-implantation embryo but develop poorly to post-implantation stages. Other models, including gastruloids, 2D micropatterns and embryoid bodies, are capable of modelling aspects of post-implantation development[21-24]. However, these models are derived entirely from hESC, lack extraembryonic tissues, and do not recapitulate embryo

bioRxiv preprint doi: https://doi.org/10.1101/2023.06.15.545082; this version posted June 15, 2023. The copyright holder for this preprint (which was not certified by peer review) is the author/funder, who has granted bioRxiv a license to display the preprint in perpetuity. It is made available under aCC-BY-NC-ND 4.0 International license.

74 morphology. A recent study, which combines epiblast-like spheroids with BMP4-treated hESCs
75 expressing a mixture of extraembryonic markers, marks a step towards integrated models of the
76 post-implantation embryo[25]. However, this model does not exhibit self-organization of an epiblast-
77 like compartment in the context of extra-embryonic tissues until after lumenogenesis, and the
78 BMP4 treated hESCs are not correlated to targeted extraembryonic lineages.
79
80 Several protocols have been developed to derive trophoblast and hypoblast cells from hESCs[26-
81 31]. Importantly, the pluripotent state influences the developmental trajectory of differentiated
82 cells[26,27]. The derivation of lineage-specific cell lines offers scope for modelling these tissues *in*
83 *vitro*. However, generating a modular, integrated model system that includes both embryonic and
84 extraembryonic tissues has proven challenging. This may be due to the opposing signaling
85 pathway modulators required for in hESC culture, hypoblast-like cell differentiation, and
86 trophoblast-like cell differentiation. Moreover, while tissue-tissue crosstalk is an advantage of
87 integrated model systems, generation of embryoids in media containing exogenous factors may
88 compromise tissue-driven self-organization. Given these limitations, and the ability of tri-lineage
89 models to mimic mouse development[32-34], we utilized the approach of overexpressing
90 transcription factors that can drive generation of extraembryonic-like cells without the need for
91 exogenous factors.
92
93 We show that aggregates of induced extraembryonic-like lineages and wildtype hESC are
94 capable of self-organisation into embryo-like structures, which mimic several hallmarks of post-
95 implantation development, including lumenogenesis, amniogenesis, primordial germ cell
96 formation, and specification of the anterior hypoblast. Importantly, these inducible human
97 embryoids are modular, do not rely on exogenous signaling factors, and are amenable to genetic
98 perturbation.
99

bioRxiv preprint doi: https://doi.org/10.1101/2023.06.15.545082; this version posted June 15, 2023. The copyright holder for this preprint (which was not certified by peer review) is the author/funder, who has granted bioRxiv a license to display the preprint in perpetuity. It is made available under aCC-BY-NC-ND 4.0 International license.

Results

Transcription factor-mediated induction of extraembryonic lineages

Mouse ESCs can be induced to generate extraembryonic endoderm or trophoblast through expression of Gata4 or Cdx2, respectively, and these cells are capable of modelling development in a 3D embryoid models[33-35]. Thus, we first identified factors that can similarly upregulate extraembryonic gene programs in human ESC. Notably, pluripotent state, in part, dictates differentiation potential from ESCs[26,27,29,30,36]. Therefore, we overexpressed candidate transcription factors in hESCs across the pluripotency spectrum to assess which factors are able to program hESCs to trophoblast or hypoblast-like cells. We first integrated published single cell RNA-sequencing data of human embryos cultured until gastrulation[2,13,37-40] and used the computational tool SCENIC to score the predicted activity of transcription factors enriched in the epiblast, trophoblast or hypoblast to generate a putative gene regulatory network (**Extended Figure 1A**)[41]. As expected, we found that *SOX2*, *NANOG* and *POU5F1* (OCT4) showed high predicted activity in the epiblast. Transcription factors including *GATA4*, *GATA6*, *SOX17* and *FOXA2* were particularly active in the hypoblast and *GATA3*, *NR2F2*, *GATA2* and *TFAP2C* (also known as AP2γ) showed enriched activity in the trophoblast (**Extended Figures 1A-B**). The overexpression of *GATA6* or *SOX17* has been shown to drive endodermal gene programs from primed hESCs[42,43], therefore, we selected them as candidates to program hESCs to become hypoblast-like. Similarly, *GATA3* and *TFAP2C* have been reported to share high chromatin co-occupancy during differentiation of hESCs into trophoblast stem cells[44]. This, together with their high predicted activity in trophoblast, led us to select *GATA3* and *TFAP2C* as candidates to drive hESCs to become trophoblast-like. We generated hESCs with doxycycline-inducible individual or combined transgenes for the transcription factors of interest: namely *GATA6* and *SOX17* to program hESCs to hypoblast-like cells (**Figure 1A**); and *GATA3* (together with an *eGFP* also

bioRxiv preprint doi: https://doi.org/10.1101/2023.06.15.545082; this version posted June 15, 2023. The copyright holder for this preprint (which was not certified by peer review) is the author/funder, who has granted bioRxiv a license to display the preprint in perpetuity. It is made available under aCC-BY-NC-ND 4.0 International license.

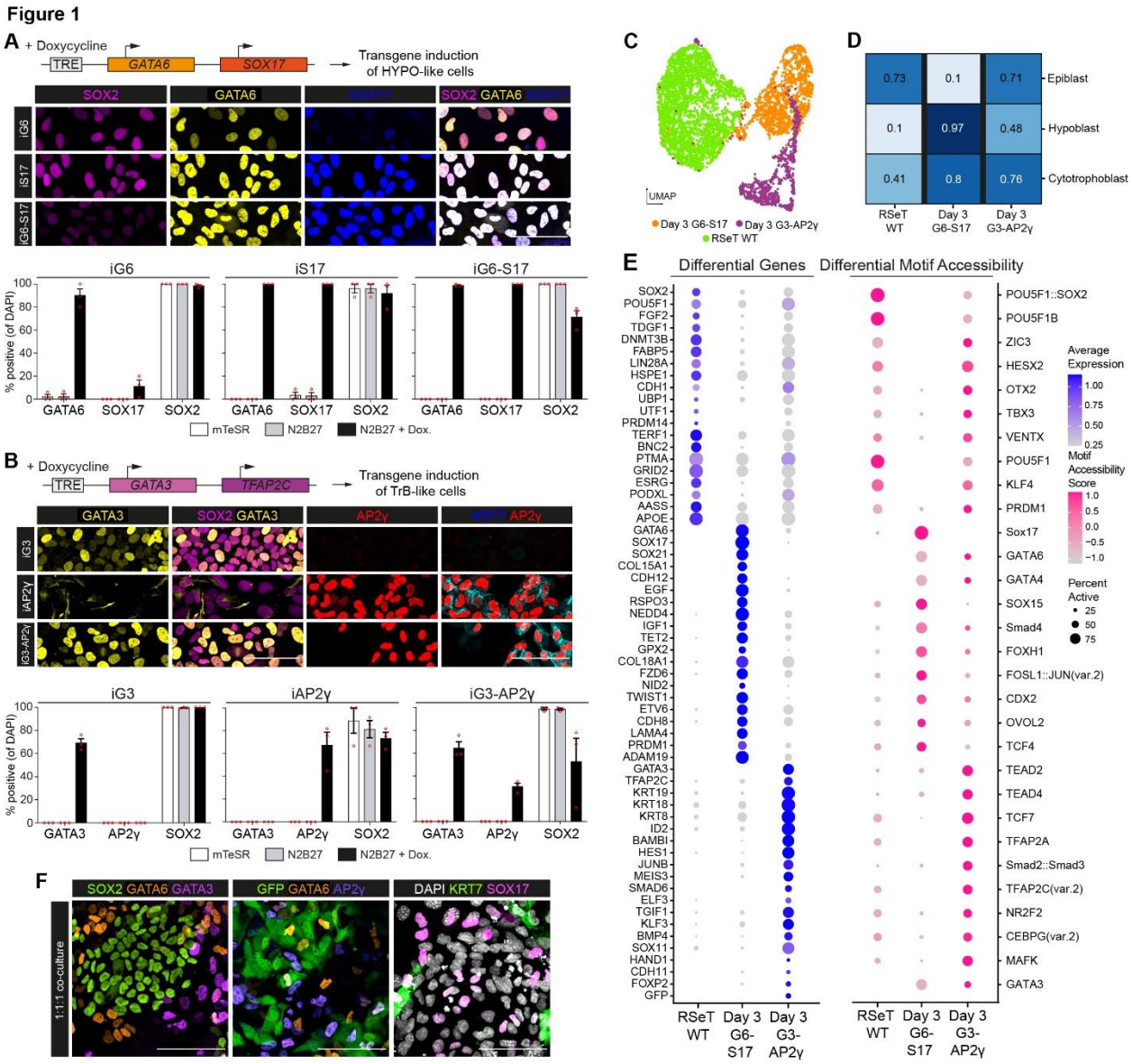

Figure 1. Validation of extraembryonic-like induction.

(A) Generation of inducible GATA6 (iG6) and/or SOX17 (iS17) hESCs and validation after 24 hours of doxycycline addition in basal N2B27. N=3 independent exerpiments with 551 iG6, 550 iS17, 707 G6-S17 cells (B) Generation of inducible GATA3 (iG3) and/or AP2γ (iAP2γ) hESCs and validation after 24 hours of doxycycline addition in basal N2B27. N=3 independent experiments with 1456 iG3, 409 iAP2γ, 782 iG3- AP2γ cells (C) Visualization of Uniform Manifold Approximation and Projection (UMAP)-based dimensional reduction of sequenced wildtype (RSeT WT), inducible GATA6-SOX17 (Day 3 iG6-S17) and inducible GATA3-AP2γ (Day 3 iG3-AP2γ) RSeT hESCs after 3 days of doxycycline induction. (D) Logistic regression analysis and comparison of cells to human post-implantation embryo populations. Cell line data projected onto human embryo data from Molè et al., 2021. (E) Selected differentially expressed genes from RNA-sequencing (blue; left) and predicted differential motif accessibility from ATAC-sequencing scored by chromVAR (pink; right) for wildtype, inducible GATA6-SOX17 and inducible GATA3-AP2γ RSeT hESCs after 3 days of doxycycline induction. (F) Validation of wildtype, inducible GATA6-SOX17 and inducible GATA3-AP2γ RSeT hESC co-culture in 2D.

124 driven by doxycycline) and *TFAP2C* to program hESCs to trophoblast-like cells (**Figure 1B**).

bioRxiv preprint doi: https://doi.org/10.1101/2023.06.15.545082; this version posted June 15, 2023. The copyright holder for this preprint (which was not certified by peer review) is the author/funder, who has granted bioRxiv a license to display the preprint in perpetuity. It is made available under aCC-BY-NC-ND 4.0 International license.

Transcription factor induction was validated following doxycycline administration for 24 hours (**Figures 1A-B**).

To assess the capacity of the selected candidate transcription factors to program hESCs to extra-embryonic-like cell identity, we overexpressed them – singly and in combination – in cells across the naïve-to-primed pluripotency spectrum. We cultured cells using three established starting conditions: PXGL, which supports pre-implantation-like naïve hESCs; RSeT, which generates intermediate peri-implantation-like pluripotent hESCs; and conventional mTeSR1 conditions to maintain post-implantation-like primed hESCs. After three days of transcription factor overexpression in basal N2B27 media, we observed significant differences in extraembryonic gene induction using both individual or combined transgenes and starting from different pluripotency states, at both the protein and mRNA level (**Extended Figure 1C-D, Extended Figure 2**). In hypoblast-like cell induction, GATA6 overexpression did not drive SOX17 expression after 3 days of induction in N2B27 from RSeT or PXGL conditions, but SOX17 overexpression resulted in robust GATA6 upregulation across starting pluripotency state conditions (**Extended Figure 1C, 2A-B**). FOXA2 expression was consistently upregulated after combined GATA6 and SOX17 induction from primed and RSeT, but not from PXGL conditions (**Extended Figure 2A-B**). These data indicate that while GATA6 and SOX17 can indeed drive endodermal gene programs, the regulation of specific downstream targets differs depending on the initial pluripotency state.

The AP2γ transgene appeared particularly effective in upregulating GATA2 and CK7 expression when driving trophoblast-like cell formation. However, induction of AP2γ alone resulted in cell death and loss of transgene expression in primed, but not RSeT or PXGL, cells (**Extended Figure 2C-D**). Combined induction of GATA6 and SOX17 or GATA3 and AP2γ resulted in consistent

bioRxiv preprint doi: https://doi.org/10.1101/2023.06.15.545082; this version posted June 15, 2023. The copyright holder for this preprint (which was not certified by peer review) is the author/funder, who has granted bioRxiv a license to display the preprint in perpetuity. It is made available under aCC-BY-NC-ND 4.0 International license.

downregulation of pluripotency markers, including NANOG, SOX2 and OCT4 (**Extended Figure 1C-D, Extended Figure 2A-D)**.

We hypothesized that RSeT hESCs are the best starting cell type to generate our stem cell-derived human post-implantation embryo model because they: (1) represent a peri-implantation stage of development[27]; (2) express low levels of amnion-specific genes during trophoblast-like cell induction compared to primed cells (**Extended Figure 1D, Extended Figure 2C-D**); and (3) are known to more readily differentiate to peri- and post-implantation yolk sac-like endoderm cells as compared to PXGL cells[26,27]. For these reasons, and the synergistic action of dual induction of candidate transcription factors, we used RSeT hESCs with inducible GATA6 and SOX17 transgenes for hypoblast-like cell induction and used cells with inducible GATA3 and AP2γ transgenes for trophoblast-like cell induction in subsequent experiments. We compared transcription factor overexpression-based induction of extraembryonic gene programs to established exogenous factor-based hypoblast-like cell and trophoblast-like cell directed differentiation protocols. Dual induction of GATA6 and SOX17 from RSeT cells in basal media induced endodermal gene expression equivalent to directed differentiation protocols in yolk sac-like cell differentiation conditions (Activin-A, CHIR99021, and LIF) (**Extended Figures 3A-B**). Dual induction of GATA3 and AP2γ from RSeT cells in basal media induced trophoblast gene expression, albeit at varying levels when compared to directed trophoblast differentiation protocols using MEK/ERK inhibition (PD0325901) and ALK5/7 inhibition (A83-01) with or without Hippo signaling pathway inhibition (lysophosphatidic acid; LPA) (**Extended Figures 3C-D**).

To further characterize RSeT hESCs induced to express GATA6-SOX17 or GATA3-AP2γ, we carried out single-cell 10x multiome sequencing and assessed transcriptomic and chromatin accessibility simultaneously. When this single-cell data was visualized using uniform manifold

bioRxiv preprint doi: https://doi.org/10.1101/2023.06.15.545082; this version posted June 15, 2023. The copyright holder for this preprint (which was not certified by peer review) is the author/funder, who has granted bioRxiv a license to display the preprint in perpetuity. It is made available under aCC-BY-NC-ND 4.0 International license.

approximation and projection (UMAP), cells clustered based on cell type (**Figure 1C**), and the application of a logistic regression framework showed that the wildtype, inducible GATA6-SOX17, and inducible GATA3-AP2γ RSeT hESCs had the highest similarities to the epiblast, hypoblast, and cytotrophoblast of the post-implantation embryo, respectively (**Figure 1D**). Analysis of differentially expressed genes and differentially accessible motifs scored by chromVAR[45] revealed similar embryonic and extraembryonic dynamics (**Figure 1E, Extended Figure 4, Extended Table 1**). Specifically, we detected enriched expression and motif accessibility scores of pluripotency and epiblast markers in RSeT hESCs (*SOX2*, *POU5F1*, *TDGF1*); of hypoblast markers in GATA6-SOX17 inducible cells (*RSPO3*, *IGF1*, *PRDM1*); and of trophoblast markers (*KRT19, KRT18, BMP4*), including Hippo, WNT and TGFβ pathway components in the GATA3-AP2γ inducible cells. Together, these data demonstrate that transcription factor-mediated induction of extraembryonic cell fate from RSeT hESCs readily drives hypoblast- or trophoblast-like gene programs without the need for exogenous factors. This allows us to overcome the challenge presented for successful coculture of these cell types by their conflicting culture media requirements. Indeed, 1:1:1 co-culture of wildtype RSeT hESCs with inducible GATA6-SOX17 and inducible GATA3-AP2γ RSeT hESCs demonstrated good survival and mixed identity after transgene induction for 3 days **(Figure 1F**).

Self-assembly of a tri-lineage 3D post-implantation model

As all three RSeT hESC-derived cell types – wildtype, GATA6-SOX17 inducible and GATA3-AP2γ inducible – can be cocultured in N2B27 medium, we induced expression of the selected transcription factors with doxycycline for 3 days to generate hypoblast- and trophoblast-like cells and subsequently aggregated cell mixtures in Aggrewell dishes (**Figure 2A**).

bioRxiv preprint doi: https://doi.org/10.1101/2023.06.15.545082; this version posted June 15, 2023. The copyright holder for this preprint (which was not certified by peer review) is the author/funder, who has granted bioRxiv a license to display the preprint in perpetuity. It is made available under aCC-BY-NC-ND 4.0 International license.

Figure 2

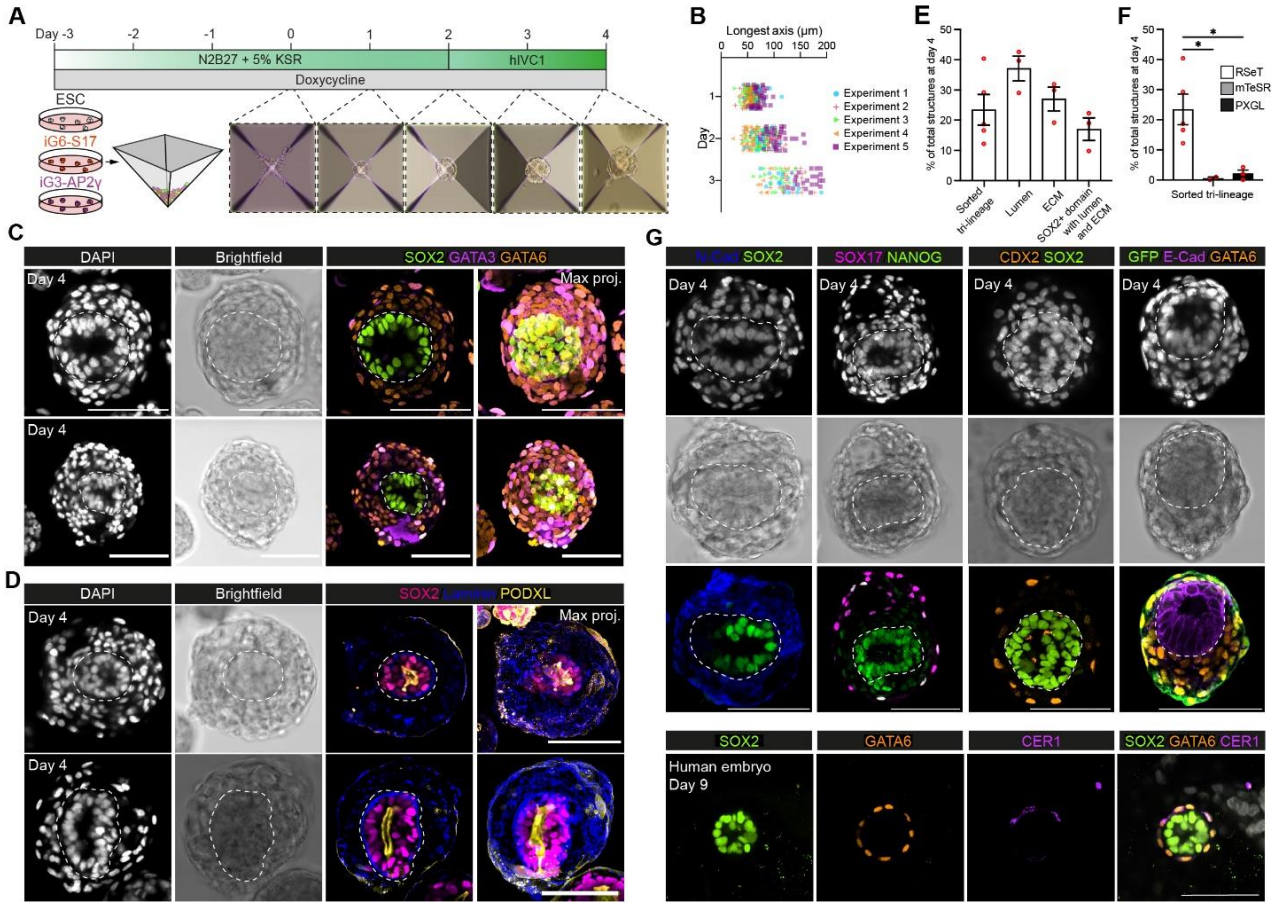

Figure 2. Generation of inducible post-implantation human embryoids

(A) Overview of experimental protocol to generate inducible human embryoids by combining wildtype RSeT hESC with inducible extraembryonic-like cells. To generate hypoblast-like cells, inducible GATA6-SOX17 (iG6-S17) was used. To generated trophoblast-like cells, inducible GATA3-AP2γ (iG3-AP2γ) was used. Extraembryonic-like cells were induced for 3 days before aggregation at Day 0. (B) Size of cell aggregates between day 1 to day 3 following aggregation. N=5 independent experiments with 175 day 1, 171 day 2, and 91 day 3 structures. (C) At 96 hours after aggregation, structures demonstrate clear self-organization with an inner SOX2-positive domain surrounded by sequential layers of GATA6-positive and GATA3-positive extraembryonic-like populations. (D) Inducible human embryoids demonstrate clear apicobasal polarity within the inner SOX2-positive domain, including PODXL-positive lumen formation and basal deposition of laminin between the SOX2-positive epiblast-like and hypoblast-like compartments. (E) Quantification of inducible human embryoid formation efficiency and organization. N=5 indpedent experiments with 952 structures for tri-lineage, 3 independent experiments with 506 structures for lumen and ECM efficiency. (F) Quantification of inducible human embryoid formation across starting pluripotency states. N=5 independent experiments with 1189 structures quantified. (G) The hypoblast-like domain expresses N-Cadherin and SOX17. Cells derived from inducible GATA3-AP2γ (which expresses GFP) show clear outer localization. (H) Representative image of an in vitro cultured human embryo at 9 days post-fertilization showing clear lumenized SOX2 domain surrounded by a layer of GATA6-postive cells. A subset of GATA6-positive cells expresses the anterior hypoblast marker CER1. Scale bars = 100mm. Statistics: (F) one-way ANOVA with Dunnett's multiple comparisons test. *p<0.05.

We plated a ratio of 1:1:2 wildtype:GATA6-SOX17-inducible:GATA3-AP2γ-inducible cells with 3.6 x 10^4 cells per Aggrewell-400 24-well in N2B27 media (approximately 8:8:16 cells per microwell).

bioRxiv preprint doi: https://doi.org/10.1101/2023.06.15.545082; this version posted June 15, 2023. The copyright holder for this preprint (which was not certified by peer review) is the author/funder, who has granted bioRxiv a license to display the preprint in perpetuity. It is made available under aCC-BY-NC-ND 4.0 International license.

Cells aggregated within 24 hours, and by 48 hours post-aggregation we observed clear distinctions between inner and outer cellular domains by brightfield (**Figure 2A**). At 48 hours post-aggregation, the media was changed to post-implantation human embryo media (hIVC1)[2,12,13]. Incubation with doxycycline continued throughout the whole period of culture (**Figure 2A**). Cells aggregated and proliferated consistently across experiments (**Figure 2B**). Four days post-aggregation, the cell aggregates had self-organized into structures with a SOX2-positive, epiblast-like domain containing a central lumen; an outer single layer of GATA3-positive putative trophoblast-like cells; and an intermediate putative hypoblast-like domain of GATA6-positive cells between inner lumenized domain and outer layer (**Figure 2C**). The inner SOX2-positive domain exhibited apicobasal polarity with apical expression of the luminal marker PODXL, and basal deposition of laminin (**Figure 2D**). Similar to experiments in which mouse embryonic and extraembryonic stem cells were aggregated to generate a post-implantation mouse embryo model, these structures did not transit through a blastocyst-like morphology prior to forming post-implantation-like structures[32-34,46-48]. The efficiency of inducible human embryoid formation (defined as aggregates containing an organized SOX2-positive domain, surrounded by concentric layers of GATA6-positive and GATA3-positive cells) was approximately 23% (**Figure 2E**). By contrast, when using primed mTeSR1 or naïve PXGL hESCs as the starting pluripotency state for constitutive wildtype, GATA6-SOX17 inducible, and GATA3-AP2γ inducible cells, the efficiency of organized, multi-lineage structure formation was less than 5% (**Figure 2F**).

Our inducible human embryoids expressed several other lineage markers in an organized manner, including N-Cadherin and SOX17 in the putative hypoblast-like compartment and CDX2 in the outer layer of putative trophoblast-like cells (**Figure 2G**). We also observed structures with SOX17 and/or GATA6 expression within outer GATA3-AP2γ-induced cells (marked by eGFP), which may reflect the reported tendency of peripheral cells to adopt endodermal identities in

bioRxiv preprint doi: https://doi.org/10.1101/2023.06.15.545082; this version posted June 15, 2023. The copyright holder for this preprint (which was not certified by peer review) is the author/funder, who has granted bioRxiv a license to display the preprint in perpetuity. It is made available under aCC-BY-NC-ND 4.0 International license.

embryoid bodies[49,50]. The epiblast-like inner compartment expressed SOX2, NANOG and E-Cadherin and maintained pluripotent and epithelial identity akin to the human embryo (**Figure 2G**). These data demonstrate that RSeT hESC-derived epiblast-, hypoblast- and trophoblast-like cells are able to self-organize into embryo-like structures reminiscent of the post-implantation human embryo at 8-9 days post-fertilization (**Figure 2H**).

Generation of amnion, primordial germ cells, and extra-embryonic mesenchyme

To gain insight into whether our human embryo model develops gene expression and chromatin accessibility patterns that align to the natural human embryo, we performed single-cell multiome RNA and ATAC sequencing on human embryo models at 4, 6, and 8 days post-aggregation (**Figure 3A**). We selected individual structures for sequencing based on their development of the three tissues: (1) an inner, epithelial domain; (2) an intermediate domain surrounding the central epithelium; and (3) an outer GFP-positive cell layer (**Extended Figure 5A**). We used these criteria because these structures represented self-organized stem cell-derived aggregates that resembled aspects of the post-implantation human embryo. After quality control to filter out cell barcodes with low mapped reads to either RNA or chromatin, 5217 cells were included in the analysis spanning all three timepoints (**Figure 3B**). To assign clusters without bias, we used scmap[51] to project our dataset onto human[2,52] and cynomolgus macaque[53-55] datasets spanning peri-implantation to gastrula stages (**Figure 3B and Extended Figure 5B**). This analysis allowed us to project gene expression signatures from previously annotated cynomolgus macaque cell type clusters including epiblast-, amnion-, visceral endoderm-, extraembryonic mesenchyme- and gastrulation-like populations onto our human embryo model. The recently published multiome-based velocity inference program multivelo[56] was used to predict lineage relationships from combined RNA and chromatin velocity measurements. We found that the inferred differentiation time correlated well with the transition of structures from day 4 to day 8 post-aggregation. These data, in combination with canonical marker expression, allowed us to annotate the cell types in

bioRxiv preprint doi: https://doi.org/10.1101/2023.06.15.545082; this version posted June 15, 2023. The copyright holder for this preprint (which was not certified by peer review) is the author/funder, who has granted bioRxiv a license to display the preprint in perpetuity. It is made available under aCC-BY-NC-ND 4.0 International license.

our human embryo model (**Figure 3B and Extended Figure 5C**). We identified clusters resembling embryonic late-epiblast (L-EPI: *TDGF1, SOX2, NANOG*-positive), amnion (AM-1: *TFAP2A, ID1*-positive; AM-2: *ISL1, TFAP2C*-positive; and AM-3: *GABRP, VTCN1, GRHL1, MEIS1*-positive), mesoderm (MESO-1: *TBXT*+, *MESP1*-positive; MESO-2: *MIXL1, CER1, SNAI1, EOMES*-positive), extraembryonic mesenchyme (EXMC: *POSTN, COL6A3, IGF2, TBX20*-positive) and hypoblast/visceral endoderm (HYPO/VE: *BMP6, CDH2, HNF1B, FOXA2*-positive) (**Figure 3C and Extended Figure 5C-D**). We did not identify a distinct trophoblast-like cluster derived from the GFP-positive inducible GATA3-AP2γ cells, despite their presence as an outer layer within the inducible human embryoids (**Figure 3A, Extended Figure 5E**). Given the aberrant upregulation of endodermal markers after aggregation, inducible GATA3-AP2γ-derived cells were not likely to represent *bona fide* trophoblast. Nevertheless, these inducible human embryoids generated several cell types which do not appear to be formed when human embryos are cultured *in vitro* through implantation, including amnion and extraembryonic mesenchyme. This is in agreement with immunofluorescence analysis that demonstrated that the inner, SOX2-positive domain exited pluripotency by day 6 post-aggregation and upregulated amnion markers, including CDX2 and ISL1. In addition, by day 8 post-aggregation, the inner domain upregulated mature amnion markers VTCN1 and HAND1 (**Figure 3D, Extended Figure 6A-B**). The GATA6-positive domain also co-expressed HAND1, supporting the presence of extraembryonic mesenchyme (**Extended Figure 6A-B**). A subset of GATA6-positive cells showed high co-expression of FOXF1 or TBX20, highlighting the two populations within the intermediate domain of our human embryo model: hypoblast cells (GATA6-positive, FOXF1 or TBX20-low) and extraembryonic mesenchyme (GATA6-positive, FOXF1 or TBX20-high) (**Extended Figure 6C-F**).

bioRxiv preprint doi: https://doi.org/10.1101/2023.06.15.545082; this version posted June 15, 2023. The copyright holder for this preprint (which was not certified by peer review) is the author/funder, who has granted bioRxiv a license to display the preprint in perpetuity. It is made available under aCC-BY-NC-ND 4.0 International license.

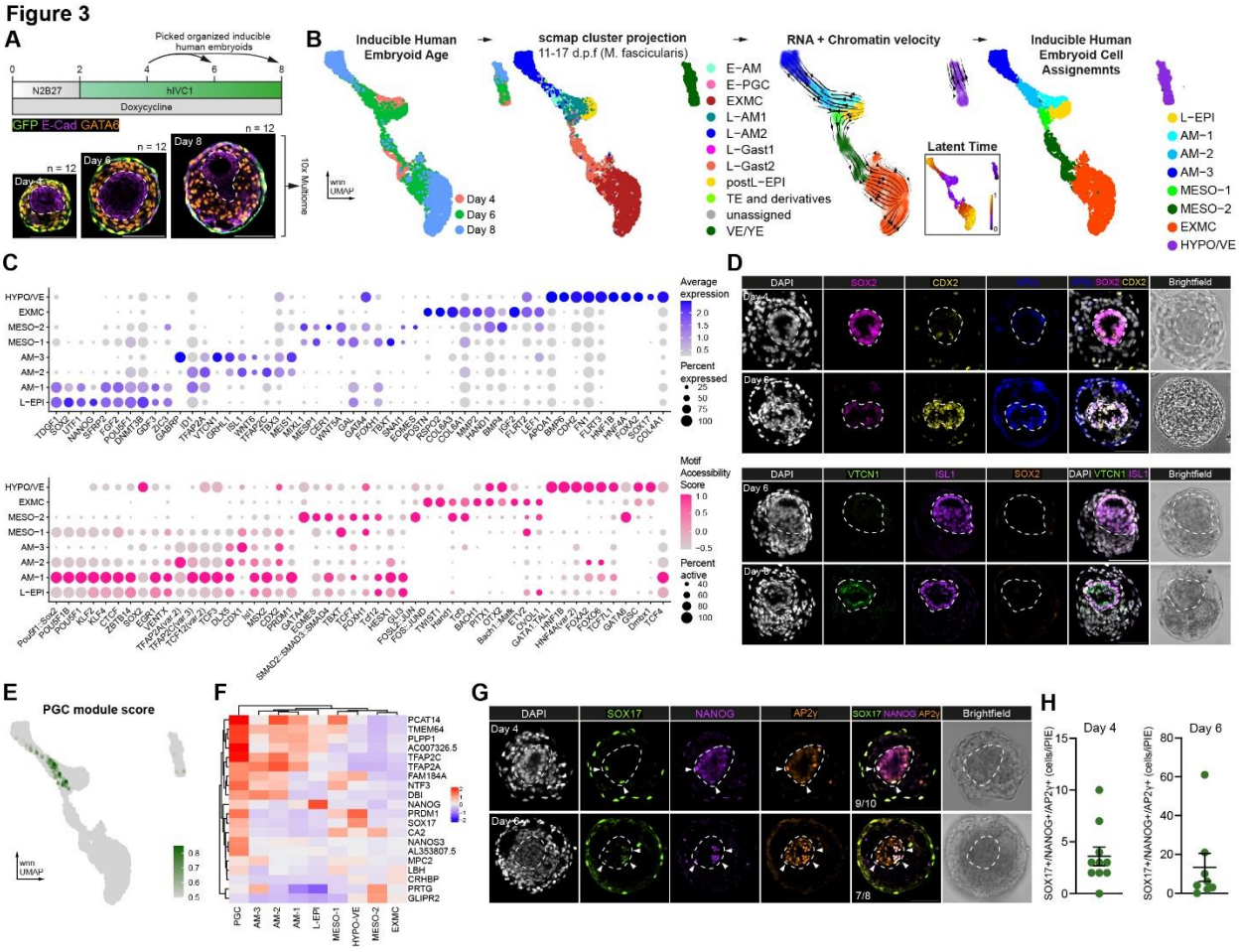

Figure 3. Differentiation of extraembryonic mesenchyme, amnion, and primordial germ cells.

(A) Schematic of extended culture protocol of inducible human embryoids and sampling for combined single-cell RNA and single-cell ATAC sequencing using the 10x platform. (B) Cells were annotated based on transcriptional projection to multiple human and non-human primate embryo datasets using scmap in conjunction with RNA and chromatin velocity. (C) Selected differentially expressed genes in the RNA-sequencing data (top, blue) and predicted differentially accessible motifs scored by chromVAR on the ATAC-sequencing data (bottom, pink) across clusters. (D) Inducible human embryoids downregulated SOX2 and upregulated CDX2, ISL1 at day 6 and VTCN1 at day 8, indicative of robust amnion differentiation and maturation. (E) Module scoring for primordial germ cell marker genes (Jo et al., 2021). (F) Heatmap of selected primordial germ cell genes across clusters. (G) Immunofluorescence identification of SOX17/NANOG/AP2γ triple-positive primordial germ cell-like cells in inducible human embryoids highlighted by arrowheads. (H) Quantification of SOX17/NANOG/AP2γ triple-positive (+) cells at days 4 (n=10 embryoids) and 6 (n=10 embryoids). N=2 independent experiments. Scale bars = 100μm.

Recent reports have postulated that both amnion and primordial germ cells, the precursors to gametes, are at least partially generated from a bipotent progenitor *in vitro*[57-59]. We therefore asked whether such progenitors or their progeny were specified in our human embryo model. We first assigned a primordial germ cell module score based on expression of genes identified in human primordial germ cell-like cells differentiated *in vitro*[60]. We could identify cells with

bioRxiv preprint doi: https://doi.org/10.1101/2023.06.15.545082; this version posted June 15, 2023. The copyright holder for this preprint (which was not certified by peer review) is the author/funder, who has granted bioRxiv a license to display the preprint in perpetuity. It is made available under aCC-BY-NC-ND 4.0 International license.

transcriptomes resembling primordial germ cell-like cells mostly throughout the amnion clusters AM-1, AM-2, and a small number within the mesodermal cluster MESO-1 **Figure 3E**). Putative primordial germ cell-like cells in inducible human embryoids expressed *TFAP2A* (also known as AP2α), a crucial marker of bipotent amnion and primordial germ cell-like cell progenitors[57-59]. In contrast to other cells in AM-1 and AM-2 clusters, primordial germ cell-like cells expressed the pluripotency marker *NANOG* and primordial germ cell markers *PRDM1* (also known as BLIMP1) and *NANOS3* (**Figure 3F**). Immunofluorescence analysis of a canonical set of human primordial germ cell markers[57] confirmed that SOX17/NANOG/AP2γ triple-positive primordial germ cell-like cells were observed by day 4 post-aggregation and increased in number by day 6 post-aggregation (**Figures 3G-H**). These data demonstrate that our human embryo model specifies *bona fide* germ cells. This primordial germ cell-like cell specification is concomitant with amnion-like cell formation and occurs within the inner epiblast-like compartment, supporting the existence of a bipotent progenitor for these two lineages.

The epiblast-like domain differentiates to amnion and extraembryonic mesenchyme in response to BMP signaling

Both amnion and extraembryonic mesenchyme are thought to arise in response to BMP signaling in the primate embryo[8,53,61,62]. To understand if this is consistent in our human embryo model, we examined the expression of downstream BMP response genes *ID1-4*[63]. *ID1* and *ID4* were upregulated during amnion formation, while *ID3* and *ID2* were enriched in both amnion and extraembryonic mesenchyme trajectories, indicating that BMP signaling was likely active (**Figure 4A**)[63]. In support of this, SMAD5 motif accessibility based on the ATAC-sequencing (scored by chromVAR[45]) was high in both trajectories while SMAD2::SMAD3::SMAD4 motif accessibility score, a downstream target of Activin-NODAL signaling, was not (**Figure 4B**). In line with this observation, a high BMP and low NODAL signaling environment has been implicated recently in amnion differentiation of marmoset ESCs[64] and in hESC to extraembryonic mesenchyme

bioRxiv preprint doi: https://doi.org/10.1101/2023.06.15.545082; this version posted June 15, 2023. The copyright holder for this preprint (which was not certified by peer review) is the author/funder, who has granted bioRxiv a license to display the preprint in perpetuity. It is made available under aCC-BY-NC-ND 4.0 International license.

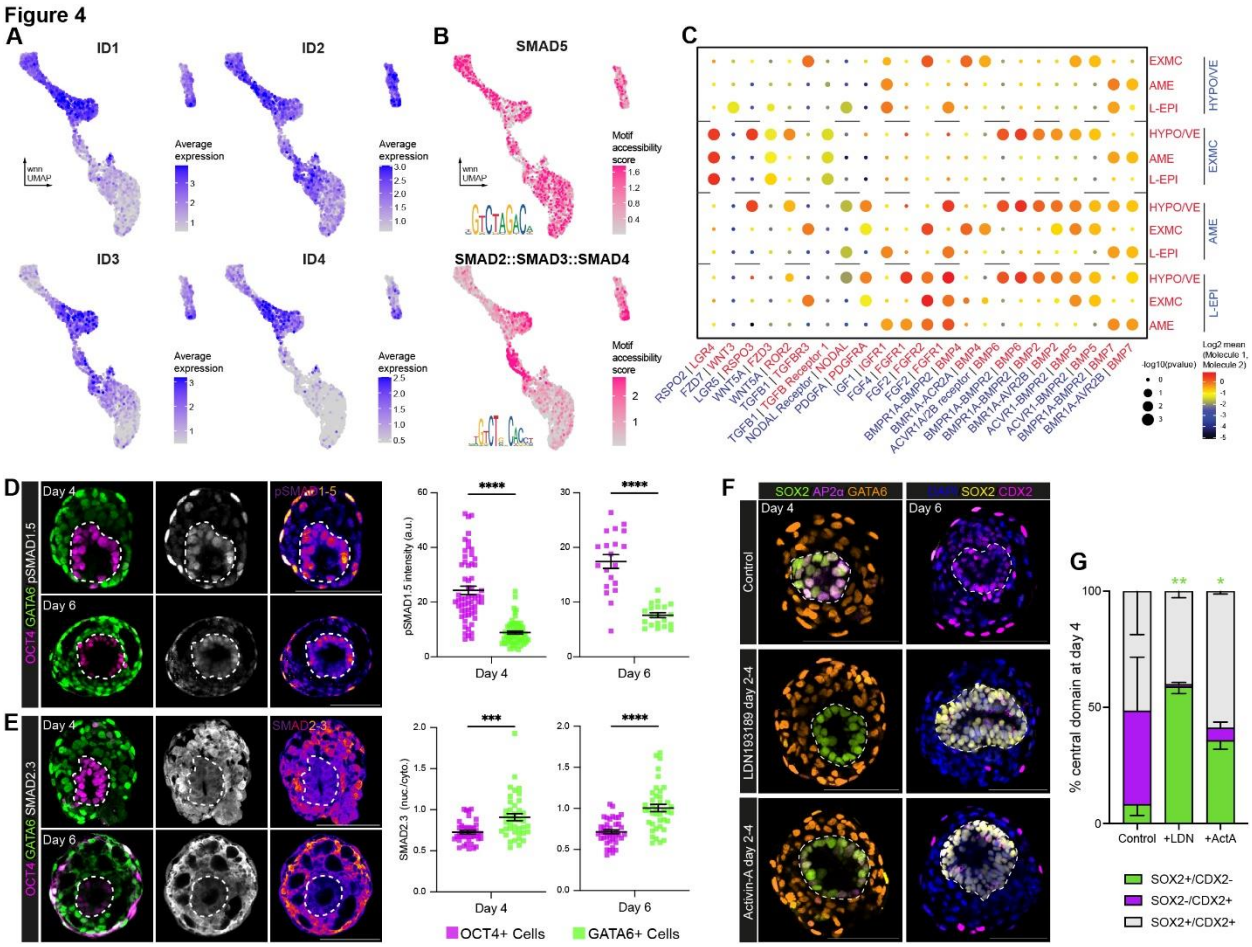

Figure 4. BMP signaling drives amnion specification in inducible human embryoids.

(A) Expression of *ID1*, *ID2*, *ID3* and *ID4* transcripts, downstream targets of BMP signaling, in sequencing of post-implantation embryo models. (B) chromVAR-based motif accessibility scores of SMAD5 and SMAD2::SMAD3::SMAD4, effectors of BMP and NODAL signaling, respectively. (C) Predicted ligand-receptor pairings in inducible human embryoids generated by CellPhoneDB (Efremova et al., 2020). (D) Representative immunofluorescence staining and quantification of representative inducible human embryoids at days 4 (n=120 cells) and 6 (n=80 cells) showing heightened pSMAD1.5 in the epiblast-like domain. N=3 independent experiments (E) Representative immunofluorescence staining and quantification of SMAD2.3 in representative inducible human embryoids at days 4 (n=80 cells) and 6 (n=80 cells). N=2 independent experiments. (F) Inhibition of BMP signaling blocks exit from pluripotency and upregulation of amnion markers AP2α and CDX2. (G) Quantification of the percentage of inner domains experessing SOX2 and CDX2 at day 4 (n=1088 structures from 3 indpendent experiments). Statistics: (D-E) Paired T-Test (G) RM two-way ANOVA with Sidak's multiple comparisons test. *p<0.05, **p<0.01, ***p<0.001, ****p<0.0001.

differentiation[62], suggesting that similar dynamics may drive differentiation of these populations within inducible human embryoids.

To further understand potential tissue-tissue crosstalk in our human embryo model, we used the computational tool CellPhoneDB[65] to predict ligand-receptor pairing across clusters in our single

bioRxiv preprint doi: https://doi.org/10.1101/2023.06.15.545082; this version posted June 15, 2023. The copyright holder for this preprint (which was not certified by peer review) is the author/funder, who has granted bioRxiv a license to display the preprint in perpetuity. It is made available under aCC-BY-NC-ND 4.0 International license.

cell sequencing data (**Figure 4C, Extended Figure 7A-B**). This analysis uses the expression of curated receptor-ligand pairs across clusters to score potential tissue-tissue crosstalk. CellPhoneDB predicted that hypoblast cluster-derived BMP2/6 and extraembryonic mesenchyme-secreted BMP4 were likely mediators of tissue-tissue crosstalk, and thus potentially drivers of cell differentiation. In contrast, predicted NODAL signaling between tissues was low, further supporting the presence of a high BMP, low NODAL signaling environment in the human embryo model. When CellPhoneDB was applied to the single cell sequencing data of the three cell lines aggregated to generate the embryo model (wildtype, inducible GATA6-SOX17 and inducible GATA3-AP2γ RSeT hESCs), the inducible GATA3-AP2γ cells were predicted to be the initial source of BMP (**Extended Figure 7C**). Despite the lack of distinct trophoblast-like cells in the inducible human embryoids at later stages, aggregation of inducible GATA6-SOX17 and wildtype RSeT hESC alone (i.e. without inducible GATA3-AP2γ cells) resulted in failure to form organized structures (**Extended Figure 7D**).

To verify whether BMP signaling has an active role in the differentiation of the inner domain of the embryo model, we examined phosphorylated (p)SMAD1.5 expression. pSMAD1.5 enrichment in the OCT4-positive epiblast-like domain at days 4 and 6 post-aggregation was indicative of active BMP signaling (**Figure 4D**). This was in contrast to the low nuclear/cytoplasmic ratio of total SMAD2.3, reflecting low NODAL signaling, in the epiblast-like domain (**Figure 4E**). These findings accord with the CellPhoneDB predictions. To functionally validate the role of BMP signaling in the differentiation of the inner domain, we treated the human embryo model with the ALK1/2/3/6 (BMP receptors) inhibitor LDN193189 between 48- and 96-hours post-aggregation. LDN193189 treated structures exhibited increased maintenance of SOX2 expression in the inner domain and lesser CDX2 and AP2α upregulation at day 4 and day 6 post-aggregation, compared to untreated control structures. Supplementation with Activin-A, an agonist of SMAD2.3 signaling, resulted in a similar

bioRxiv preprint doi: https://doi.org/10.1101/2023.06.15.545082; this version posted June 15, 2023. The copyright holder for this preprint (which was not certified by peer review) is the author/funder, who has granted bioRxiv a license to display the preprint in perpetuity. It is made available under aCC-BY-NC-ND 4.0 International license.

phenotype, though to a lesser degree (**Figure 4F-G**, **Extended Figure 7E**). These data demonstrate that the high levels of BMP activity and low levels of NODAL are key drivers of epiblast to amnion differentiation within the inner epithelial compartment of inducible human embryoids.

Prolonged SOX17 overexpression inhibits formation of the anterior hypoblast

BMP signals are localized to the posterior of the embryo by the antagonistic action of the anterior hypoblast, which secretes inhibitors of BMP, WNT and NODAL, including CER1 and LEFTY1[2]. We have recently demonstrated that these markers of the anterior hypoblast are expressed in peri- and post-implantation human embryos cultured *in vitro*[2]. Examination of hypoblast-like cells in our inducible human embryoids revealed that neither *CER1* nor *LEFTY1* were meaningfully expressed in the HYPO/VE single cell sequencing cluster (**Figure 5A**). We therefore reanalyzed our previously published 10x single-cell RNA sequencing data from post-implantation human embryos and the previously scored transcription factor activity. This analysis revealed that SOX17 regulon activity was enriched in the *CER1*-negative hypoblast subcluster in post-implantation human embryos (**Figure 5B**)[2]. Indeed, induction of SOX17 singly or in combination with GATA6 resulted in decreased capacity to upregulate *CER1,* as compared with GATA6 overexpression alone (**Extended Figure 1C**). To test whether single induction of GATA6 changed the constitution of hypoblast-like cell subpopulations in our human embryo model, we generated hypoblast-like cells by either inducing GATA6 expression alone or in combination with SOX17. Embryoids generated with inducible GATA6 cells at day 4 post-aggregation exhibited an increased proportion of CER1-positive cells compared to embryoids generated with inducible GATA6-SOX17 cells (**Figure 5C**). By day 6 post-aggregation, CER1 expression had decreased in structures generated with GATA6-induced cells (**Extended Figure 8A**). However, the transient presence of CER1-positive anterior hypoblast-like cells functionally impacted the epiblast-like domain. Structures generated using hypoblast-like cells with single GATA6 induction showed a higher proportion of

bioRxiv preprint doi: https://doi.org/10.1101/2023.06.15.545082; this version posted June 15, 2023. The copyright holder for this preprint (which was not certified by peer review) is the author/funder, who has granted bioRxiv a license to display the preprint in perpetuity. It is made available under aCC-BY-NC-ND 4.0 International license.

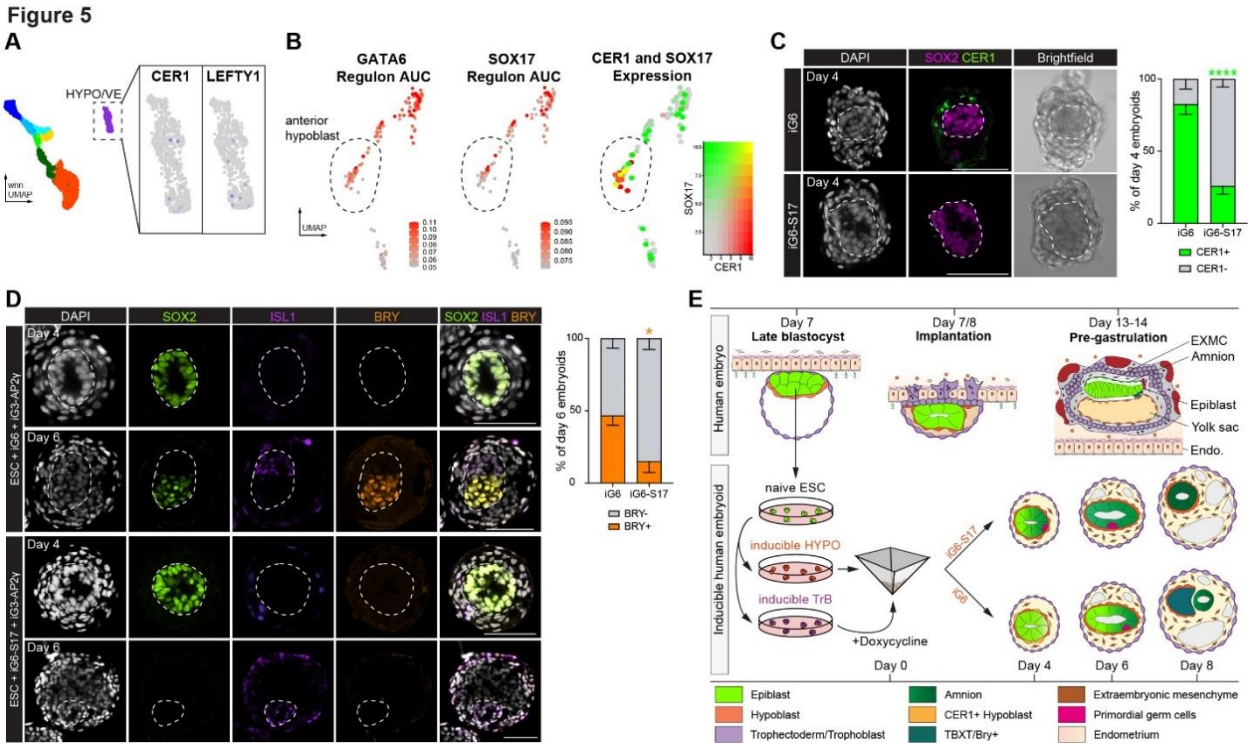

Figure 5. SOX17 induction is antagonistic to specification of the anterior hypoblast.

(A) Expression of *CER1* and *LEFTY1* in the HYPO/VE cluster of sequenced inducible human embryoids. (B) Analysis of GATA6 and SOX17 regulon activity scored by SCENIC and *SOX17* and *CER1* co-expression in the hypoblast of post-implantation human embryos (9-11 days post-fertilization). Data from Molé et al. (C) Representative examples of inducible human embryoids and quantification showing CER1-positive cells surrounding the epiblast-like domain generated using induced GATA6 (iG6) but not induced GATA6-SOX17 (iG6-S17) dual induction of hypoblast-like cells. n=66 structures from 3 independent experiments. (D) Representative immunofluorescence staining and quantification of ISL1 and BRY/TBXT expression in inducible human embryoids generated from inducible GATA6 or inducible GATA6-SOX17 dual induction. n=29 structures from 3 independent experiments. (E) Schematic overview of inducible human embryoid formation and development compared to the human embryo. The inducible embryoids are generated by combining naïve ESCs with transgene-induced extraembryonic lineages. Embryoids self-organize and mimic aspects of human post-implantation development, including lumenogenesis, pluripotency exit, amnion and extraembryonic mesenchyme differentiation, and primordial germ cell formation. Generating embryoids with single induction of GATA6 (iG6) rather than together with SOX17 (iG6-S17) results in higher rates of anterior hypoblast differentiation, allowing for later pluripotency exit and primitive streak-like differentiation. Statistics (C-D): RM two-way ANOVA with Sidak's multiple comparisons test. *p<0.05, **p<0.01, ***p<0.001, ****p<0.0001.

inner domains containing cells expressing primitive streak marker BRY/TBXT at day 6 post-aggregation as compared to structures with GATA6-SOX17 induction (**Figure 5D**). This is likely to be in response to the transient anterior hypoblast population protecting pluripotency for a longer period in these structures compared to structures generated with inducible GATA6-SOX17 cells lacking the CER1 anterior hypoblast-like domain.

bioRxiv preprint doi: https://doi.org/10.1101/2023.06.15.545082; this version posted June 15, 2023. The copyright holder for this preprint (which was not certified by peer review) is the author/funder, who has granted bioRxiv a license to display the preprint in perpetuity. It is made available under aCC-BY-NC-ND 4.0 International license.

Together, these data highlight functional differences in the gene regulatory network underlying differentiation of hypoblast subpopulations of cells, where prolonged, high SOX17 expression is antagonistic to anterior hypoblast identity and instead promotes CER1-negative hypoblast identity. Thus, by modulating the hypoblast-like cells in inducible human embryoids, we reveal the capacity of the epiblast-like domain to upregulate primitive streak markers, demonstrating the value of this modular embryo model to study interactions between embryonic and extraembryonic tissues.

Discussion

Here, we have generated a multi-lineage stem cell-derived model of the human post-implantation embryo that undergoes lumenogenesis in its epiblast-like domain and differentiation events that reflect interactions between extraembryonic-like and embryonic-like tissues. Our human embryo model forms amnion-like cells in response to BMP signaling, which progressively mature along a trajectory conserved between primates, transitioning from AP2α-positive to ISL1- and CDX2-positive to VTCN1-positive amnion cells[54,64,66]. These induced human embryoids specify primordial germ cell-like cells, which occurs as cells progress along the amnion differentiation trajectory, likely originating from a common AP2α-positive progenitor as reported in other *in vitro* systems[57-59]. Similarly, extraembryonic mesenchyme-like cells are specified within our embryo model, which closely resemble those of the primate embryo. The origin of extraembryonic mesenchyme in the human and non-human primate embryos remains unclear[8]. Our single cell sequencing analysis suggests a trajectory from the late epiblast-like population through a mesodermal intermediate, in line with a recently reported *in vitro* extraembryonic mesenchyme differentiation protocol[54,62], data from cynomolgus macaque[54], and historical observations in rhesus macaque and human embryos[67].

bioRxiv preprint doi: https://doi.org/10.1101/2023.06.15.545082; this version posted June 15, 2023. The copyright holder for this preprint (which was not certified by peer review) is the author/funder, who has granted bioRxiv a license to display the preprint in perpetuity. It is made available under aCC-BY-NC-ND 4.0 International license.

We show that modulating the transcription factor combination used to drive hypoblast-like cell induction shifts the balance of hypoblast contribution from CER1-negative hypoblast-like cells (GATA6-SOX17 induction) towards CER1-positive anterior hypoblast-like cells (GATA6 induction alone). The presence of the anterior hypoblast-like cells at day 4 post-aggregation appears to protect epiblast-like domain pluripotency for a longer period, allowing for exit from pluripotency at a developmentally later stage. This result is in agreement with the increased expression of the primitive streak marker BRY/TBXT at day 6 post-aggregation. These results suggest that RSeT hESCs acquire the capacity to differentiate into primitive streak-like cells in the embryo model over time as reported for other naïve hESC[68]. In contrast, the prolonged induction of SOX17 (together with GATA6) in hypoblast-like cells inhibits CER1 expression, leading to the earlier upregulation of pSMAD1.5 and precocious differentiation toward amnion and extraembryonic mesenchyme fates. This points to the existence of a distinct intermediate pluripotent state able to give rise to both amnion and extraembryonic mesenchyme, but not to germ layer derivatives. Thus, the human embryo model we have established here might be particularly useful to study the formation of amnion and extraembryonic mesenchyme as both lineages are not established during extended *in vitro* culture of human embryos[2,9,11,13,40,69].

Here, we have driven the expression of specific transcription factors to generate the two extraembryonic cell types from pluripotent hESCs and, by combining these with the parental hESC cell line, have generated a post-implantation human embryo model. Transcription factor-mediated induction of extraembryonic cells has also been used in the generation of post-implantation stem cell-derived mouse embryo models[33,34,46]. These methods allow for simple, robust culture of extraembryonic-like cells, which can be widely adopted. In contrast to pre-implantation blastoid models, the modular generation of embryoids from their constitutive parts (e.g. epiblast-, hypoblast- and trophoblast-like populations) will be useful in interrogating the role of specific tissues and tissue-specific gene requirements. We predict that the human embryoids

bioRxiv preprint doi: https://doi.org/10.1101/2023.06.15.545082; this version posted June 15, 2023. The copyright holder for this preprint (which was not certified by peer review) is the author/funder, who has granted bioRxiv a license to display the preprint in perpetuity. It is made available under aCC-BY-NC-ND 4.0 International license.

we established here will become a complementary tool to address tissue-tissue crosstalk. However, the use of transcription factor overexpression to generate extraembryonic tissues may also lead to deficiencies in differentiation, as observed in models of mouse embryogenesis[33]. For example, while GATA3 and AP2γ induction drive trophoblast-like gene programs in 2D, this population is diminished in our human embryo model after aggregation and aberrantly co-expressed endodermal markers (including SOX17 and GATA6), potentially due to their peripheral position within the structure[49,50]. Nevertheless, the GATA3-AP2γ inducible cells are required for cell aggregation, survival and organization to form the embryoids. Strikingly, induction of downstream gene regulatory networks driving both trophoblast and hypoblast lineages differed based on the initial pluripotent state. We show that this stem cell-derived model is more easily produced using peri-implantation stage, intermediate pluripotent state RSeT hESCs rather than pre-implantation stage, naïve PXGL hESCs or post-implantation stage, primed hESCs. Generating embryo-like structures from discordant pluripotent states (e.g. induction of GATA3 and/or AP2γ in naïve PXGL hESCs combined with the other two cell types from a starting RSeT condition) may lead to better recapitulation of extraembryonic fates in the future. Of note, however, PXGL hESC require extensive capacitation *in vitro* to give rise to germ layers[68] and blastoid models generated from naïve hESCs currently fail to model post-implantation stages robustly[18-20]. Similarly, primed ESCs are described by several groups to give rise to amnion-like cells in trophoblast differentiation conditions, in contrast to naïve ESCs[29,30,69]. Thus, further work interrogating the epigenetic landscape and binding sites of these factors may be useful to improve strategies to generate *bona fide* extraembryonic cells.

In summary, we present a modular, tractable model of human post-implantation development that crucially includes both embryonic- and extraembryonic-like cells. This is a post-implantation model and therefore does not have the capacity to develop to form viable human embryos, as it cannot be implanted. These inducible human embryoids do not mimic stages beyond primitive

bioRxiv preprint doi: https://doi.org/10.1101/2023.06.15.545082; this version posted June 15, 2023. The copyright holder for this preprint (which was not certified by peer review) is the author/funder, who has granted bioRxiv a license to display the preprint in perpetuity. It is made available under aCC-BY-NC-ND 4.0 International license.

448 streak formation, nor do they contain all cell types of the gastrulation-stage embryo[3]. However,
449 the construction of these embryoids demonstrates a significant step towards generating
450 integrated models of the post-implantation human embryo to allow future mechanistic studies of
451 post-implantation development that are impossible in the real human embryo.

bioRxiv preprint doi: https://doi.org/10.1101/2023.06.15.545082; this version posted June 15, 2023. The copyright holder for this preprint (which was not certified by peer review) is the author/funder, who has granted bioRxiv a license to display the preprint in perpetuity. It is made available under aCC-BY-NC-ND 4.0 International license.

Main References

1 Rossant, J. & Tam, P. P. L. in *Developmental Cell* Vol. 57 152-165 (Cell Press, 2022).

2 Molè, M. A. *et al.* A single cell characterisation of human embryogenesis identifies pluripotency transitions and putative anterior hypoblast centre. *Nature Communications* **12** (2021). https://doi.org:10.1038/s41467-021-23758-w

3 Clark, A. T. *et al.* in *Stem Cell Reports* Vol. 16 1416-1424 (Cell Press, 2021).

4 Koot, Y. E. M., Teklenburg, G., Salker, M. S., Brosens, J. J. & Macklon, N. S. in *Biochimica et Biophysica Acta - Molecular Basis of Disease* Vol. 1822 1943-1950 (2012).

5 Macklon, N. S. Conception to ongoing pregnancy: the 'black box' of early pregnancy loss. *Human Reproduction Update* **8**, 333-343 (2002). https://doi.org:10.1093/humupd/8.4.333

6 Molè, M. A., Weberling, A. & Zernicka-Goetz, M. in *Current Topics in Developmental Biology* Vol. 136 113-138 (Academic Press Inc., 2020).

7 West, R. C. *et al.* Dynamics of trophoblast differentiation in peri-implantation–stage human embryos. *Proceedings of the National Academy of Sciences of the United States of America* **116**, 22635-22644 (2019). https://doi.org:10.1073/pnas.1911362116

8 Ross, C. & Boroviak, T. E. Origin and function of the yolk sac in primate embryogenesis. *Nature Communications* **11** (2020). https://doi.org:10.1038/s41467-020-17575-w

9 Deglincerti, A. *et al.* Self-organization of the in vitro attached human embryo. *Nature* **533**, 251-254 (2016). https://doi.org:10.1038/nature17948

10 Morris, S. A. *et al.* Dynamics of anterior–posterior axis formation in the developing mouse embryo. *Nature Communications* **3**, 673-673 (2012). https://doi.org:10.1038/ncomms1671

11 Shahbazi, M. N. *et al.* Self-organization of the human embryo in the absence of maternal tissues. *Nature Cell Biology* **18**, 700-708 (2016). https://doi.org:10.1038/ncb3347

12 Bedzhov, I., Leung, C. Y., Bialecka, M. & Zernicka-Goetz, M. In vitro culture of mouse blastocysts beyond the implantation stages. *Nature Protocols* **9**, 2732-2739 (2014). https://doi.org:10.1038/nprot.2014.186

13 Xiang, L. *et al.* A developmental landscape of 3D-cultured human pre-gastrulation embryos. *Nature* **577**, 537-542 (2020). https://doi.org:10.1038/s41586-019-1875-y

14 Ruane, P. T. *et al.* Trophectoderm differentiation to invasive syncytiotrophoblast is promoted by endometrial epithelial cells during human embryo implantation. *Human Reproduction* **37**, 777-792 (2022). https://doi.org:10.1093/humrep/deac008

15 Shahbazi, M. N. *et al.* Pluripotent state transitions coordinate morphogenesis in mouse and human embryos. *Nature* **552**, 239-243 (2017). https://doi.org:10.1038/nature24675

16 Liu, X. *et al.* Modelling human blastocysts by reprogramming fibroblasts into iBlastoids. *Nature* **591**, 627-632 (2021). https://doi.org:10.1038/s41586-021-03372-y

17 Sozen, B. *et al.* Reconstructing aspects of human embryogenesis with pluripotent stem cells. *Nature Communications* **12** (2021). https://doi.org:10.1038/s41467-021-25853-4

18 Kagawa, H. *et al.* Human blastoids model blastocyst development and implantation. *Nature* **601**, 600-605 (2022). https://doi.org:10.1038/s41586-021-04267-8

19 Yanagida, A. *et al.* Naive stem cell blastocyst model captures human embryo lineage segregation. *Cell Stem Cell* **28**, 1016-1022.e1014 (2021). https://doi.org:10.1016/j.stem.2021.04.031

20 Yu, L. *et al.* Blastocyst-like structures generated from human pluripotent stem cells. *Nature* **591**, 620-626 (2021). https://doi.org:10.1038/s41586-021-03356-y

21 Zheng, Y. *et al.* Controlled modelling of human epiblast and amnion development using stem cells. *Nature* **573**, 421-425 (2019). https://doi.org:10.1038/s41586-019-1535-2

22 Moris, N. *et al.* An in vitro model of early anteroposterior organization during human development. *Nature* **582**, 410-415 (2020). https://doi.org:10.1038/s41586-020-2383-9

23 Warmflash, A., Sorre, B., Etoc, F., Siggia, E. D. & Brivanlou, A. H. A method to recapitulate early embryonic spatial patterning in human embryonic stem cells. *Nature Methods* **11**, 847-854 (2014). https://doi.org:10.1038/nMeth.3016

24 Simunovic, M. *et al.* A 3D model of a human epiblast reveals BMP4-driven symmetry breaking. *Nature Cell Biology* **21**, 900-910 (2019). https://doi.org:10.1038/s41556-019-0349-7

25 Simunovic, M., Siggia, E. D. & Brivanlou, A. H. In vitro attachment and symmetry breaking of a human embryo model assembled from primed embryonic stem cells. *Cell Stem Cell* **29**, 962-972.e964 (2022). https://doi.org:10.1016/j.stem.2022.05.001

bioRxiv preprint doi: https://doi.org/10.1101/2023.06.15.545082; this version posted June 15, 2023. The copyright holder for this preprint (which was not certified by peer review) is the author/funder, who has granted bioRxiv a license to display the preprint in perpetuity. It is made available under aCC-BY-NC-ND 4.0 International license.

26 Linneberg-Agerholm, M. *et al.* Naïve human pluripotent stem cells respond to Wnt, Nodal and LIF signalling to produce expandable naïve extra-embryonic endoderm. *Development (Cambridge)* **146** (2019). https://doi.org:10.1242/dev.180620

27 Mackinlay, K. M. L. *et al.* An in vitro stem cell model of human epiblast and yolk sac interaction. *eLife* **10** (2021). https://doi.org:10.7554/eLife.63930

28 Io, S. *et al.* Capturing human trophoblast development with naive pluripotent stem cells in vitro. *Cell Stem Cell* **28**, 1023-1039.e1013 (2021). https://doi.org:10.1016/j.stem.2021.03.013

29 Guo, G. *et al.* Human naive epiblast cells possess unrestricted lineage potential. *Cell Stem Cell* **28**, 1040-1056.e1046 (2021). https://doi.org:10.1016/j.stem.2021.02.025

30 Dong, C. *et al.* Derivation of trophoblast stem cells from naïve human pluripotent stem cells. *eLife* **9** (2020). https://doi.org:10.7554/eLife.52504

31 Weatherbee, B. A. T., Cui, T. & Zernicka-Goetz, M. Modeling human embryo development with embryonic and extra-embryonic stem cells. *Developmental Biology* **474**, 91-99 (2021). https://doi.org:10.1016/j.ydbio.2020.12.010

32 Amadei, G. *et al.* Embryo model completes gastrulation to neurulation and organogenesis. *Nature* **610**, 143-153 (2022). https://doi.org:10.1038/s41586-022-05246-3

33 Lau, K. Y. C. *et al.* Mouse embryo model derived exclusively from embryonic stem cells undergoes neurulation and heart development. *Cell Stem Cell* **29**, 1445-1458 e1448 (2022). https://doi.org:10.1016/j.stem.2022.08.013

34 Tarazi, S. *et al.* ¬Post-Gastrulation Synthetic Embryos Generated Ex Utero from Mouse Naïve ESCs. *Cell* (2022). https://doi.org:10.1016/j.cell.2022.07.028

35 Niwa, H. & Mwalilino, L. Ensemble of old and new techniques escorts ESCs to bona fide embryo-like structures. *Cell Stem Cell* **29**, 1423-1425 (2022). https://doi.org:10.1016/j.stem.2022.09.004

36 Viukov, S. *et al.* Human primed and naive PSCs are both able to differentiate into trophoblast stem cells. *Stem Cell Reports* **17**, 2484-2500 (2022). https://doi.org:10.1016/j.stemcr.2022.09.008

37 Yan, L. *et al.* Single-cell RNA-Seq profiling of human preimplantation embryos and embryonic stem cells. *Nature Structural and Molecular Biology* **20**, 1131-1139 (2013). https://doi.org:10.1038/nsmb.2660

38 Blakeley, P. *et al.* Defining the three cell lineages of the human blastocyst by single-cell RNA-seq. *Development (Cambridge)* **142**, 3613-3613 (2015). https://doi.org:10.1242/dev.131235

39 Petropoulos, S. *et al.* Single-Cell RNA-Seq Reveals Lineage and X Chromosome Dynamics in Human Preimplantation Embryos. *Cell* **165**, 1012-1026 (2016). https://doi.org:10.1016/j.cell.2016.03.023

40 Zhou, F. *et al.* Reconstituting the transcriptome and DNA methylome landscapes of human implantation. *Nature* **572**, 660-664 (2019). https://doi.org:10.1038/s41586-019-1500-0

41 Aibar, S. *et al.* SCENIC: single-cell regulatory network inference and clustering. *Nature Methods* **14**, 1083-1086 (2017). https://doi.org:10.1038/nmeth.4463

42 Wamaitha, S. E. *et al.* Gata6 potently initiates reprograming of pluripotent and differentiated cells to extraembryonic endoderm stem cells. *Genes & Development* **29**, 1239-1255 (2015). https://doi.org:10.1101/gad.257071.114

43 Séguin, C. A., Draper, J. S., Nagy, A. & Rossant, J. Establishment of Endoderm Progenitors by SOX Transcription Factor Expression in Human Embryonic Stem Cells. *Cell Stem Cell* **3**, 182-195 (2008). https://doi.org:10.1016/j.stem.2008.06.018

44 Krendl, C. *et al.* GATA2/3-TFAP2A/C transcription factor network couples human pluripotent stem cell differentiation to trophectoderm with repression of pluripotency. *Proceedings of the National Academy of Sciences of the United States of America* **114**, E9579-E9588 (2017). https://doi.org:10.1073/pnas.1708341114

45 Schep, A. N., Wu, B., Buenrostro, J. D. & Greenleaf, W. J. chromVAR: inferring transcription-factor-associated accessibility from single-cell epigenomic data. *Nat Methods* **14**, 975-978 (2017). https://doi.org:10.1038/nmeth.4401

46 Amadei, G. *et al.* Inducible Stem-Cell-Derived Embryos Capture Mouse Morphogenetic Events In Vitro. *Developmental Cell* **56**, 366-382.e369 (2021). https://doi.org:10.1016/j.devcel.2020.12.004

47 Sozen, B. *et al.* Self-assembly of embryonic and two extra-embryonic stem cell types into gastrulating embryo-like structures. *Nature Cell Biology* **20**, 979-989 (2018). https://doi.org:10.1038/s41556-018-0147-7

bioRxiv preprint doi: https://doi.org/10.1101/2023.06.15.545082; this version posted June 15, 2023. The copyright holder for this preprint (which was not certified by peer review) is the author/funder, who has granted bioRxiv a license to display the preprint in perpetuity. It is made available under aCC-BY-NC-ND 4.0 International license.

48 Harrison, S. E., Sozen, B., Christodoulou, N., Kyprianou, C. & Zernicka-Goetz, M. Assembly of embryonic and extraembryonic stem cells to mimic embryogenesis in vitro. *Science* **356** (2017). https://doi.org:10.1126/science.aal1810

49 Zeevaert, K., Elsafi Mabrouk, M. H., Wagner, W. & Goetzke, R. Cell Mechanics in Embryoid Bodies. *Cells* **9** (2020). https://doi.org:10.3390/cells9102270

50 Abe, K. *et al.* Endoderm-specific gene expression in embryonic stem cells differentiated to embryoid bodies. *Exp Cell Res* **229**, 27-34 (1996). https://doi.org:10.1006/excr.1996.0340

51 Kiselev, V. Y., Yiu, A. & Hemberg, M. scmap: projection of single-cell RNA-seq data across data sets. *Nat Methods* **15**, 359-362 (2018). https://doi.org:10.1038/nmeth.4644

52 Tyser, R. C. V. *et al.* Single-cell transcriptomic characterization of a gastrulating human embryo. *Nature* **600**, 285-289 (2021). https://doi.org:10.1038/s41586-021-04158-y

53 Ma, H. *et al.* In vitro culture of cynomolgus monkey embryos beyond early gastrulation. *Science* **366** (2019). https://doi.org:10.1126/science.aax7890

54 Yang, R. *et al.* Amnion signals are essential for mesoderm formation in primates. *Nature Communications* **12** (2021). https://doi.org:10.1038/s41467-021-25186-2

55 Nakamura, T. *et al.* A developmental coordinate of pluripotency among mice, monkeys and humans. *Nature* **537**, 57-62 (2016). https://doi.org:10.1038/nature19096

56 Li, C., Virgilio, M. C., Collins, K. L. & Welch, J. D. Multi-omic single-cell velocity models epigenome-transcriptome interactions and improves cell fate prediction. *Nat Biotechnol* (2022). https://doi.org:10.1038/s41587-022-01476-y

57 Chen, D. *et al.* Human Primordial Germ Cells Are Specified from Lineage-Primed Progenitors. *Cell Rep* **29**, 4568-4582 e4565 (2019). https://doi.org:10.1016/j.celrep.2019.11.083

58 Castillo-Venzor, A. *et al.* Origin and segregation of the human germline. *biorxiv* (2022). https://doi.org:10.1101/2022.07.06.498671

59 Zheng, Y. *et al.* Single-cell analysis of embryoids reveals lineage diversification roadmaps of early human development. *Cell Stem Cell* **29**, 1402-1419 e1408 (2022). https://doi.org:10.1016/j.stem.2022.08.009

60 Jo, K. *et al.* Efficient differentiation of human primordial germ cells through geometric control reveals a key role for Nodal signaling. *Elife* **11** (2022). https://doi.org:10.7554/eLife.72811

61 Sasaki, K. *et al.* The Germ Cell Fate of Cynomolgus Monkeys Is Specified in the Nascent Amnion. *Developmental Cell* **39**, 169-185 (2016). https://doi.org:10.1016/j.devcel.2016.09.007

62 Pham, T. X. A. *et al.* Modeling human extraembryonic mesoderm cells using naive pluripotent stem cells. *Cell Stem Cell* **29**, 1346-1365.e1310 (2022). https://doi.org:https://doi.org/10.1016/j.stem.2022.08.001

63 Hollnagel, A., Oehlmann, V., Heymer, J., Rüther, U. & Nordheim, A. Id genes are direct targets of bone morphogenetic protein induction in embryonic stem cells. *Journal of Biological Chemistry* **274**, 19838-19845 (1999). https://doi.org:10.1074/jbc.274.28.19838

64 Munger, C. *et al.* Microgel culture and spatial identity mapping elucidate the signalling requirements for primate epiblast and amnion formation. *Development* **149** (2022). https://doi.org:10.1242/dev.200263

65 Efremova, M., Vento-Tormo, M., Teichmann, S. A. & Vento-Tormo, R. CellPhoneDB: inferring cell–cell communication from combined expression of multi-subunit ligand–receptor complexes. *Nature Protocols* **15**, 1484-1506 (2020). https://doi.org:10.1038/s41596-020-0292-x

66 Bergmann, S. *et al.* Spatial profiling of early primate gastrulation in utero. *Nature* (2022). https://doi.org:10.1038/s41586-022-04953-1

67 Luckett, W. P. Origin and differentiation of the yolk sac and extraembryonic mesoderm in presomite human and rhesus monkey embryos. *Am J Anat* **152**, 59-97 (1978). https://doi.org:10.1002/aja.1001520106

68 Rostovskaya, M., Stirparo, G. G. & Smith, A. Capacitation of human naïve pluripotent stem cells for multi-lineage differentiation. *Development (Cambridge)* **146** (2019). https://doi.org:10.1242/dev.172916

69 Chhabra, S. & Warmflash, A. BMP-treated human embryonic stem cells transcriptionally resemble amnion cells in the monkey embryo. *Biology Open* **10** (2021). https://doi.org:10.1242/bio.058617

bioRxiv preprint doi: https://doi.org/10.1101/2023.06.15.545082; this version posted June 15, 2023. The copyright holder for this preprint (which was not certified by peer review) is the author/funder, who has granted bioRxiv a license to display the preprint in perpetuity. It is made available under aCC-BY-NC-ND 4.0 International license.

Tables

Table 1: List of primary antibodies used in this study

Target	Species	Company	Catalogue #	RRID
AP2-alpha	Mouse	Santa Cruz Biotechnology	sc-12726	AB_667767
AP2-gamma	Goat	R&D Systems	AF5059	AB_2255891
Brachyury	Goat	R&D Systems	AF2085	AB_2200235
CDX2	Mouse	BioGenex	MU392-UC	AB_2335627
Cerberus 1	Goat	R&D Systems	AF1075	AB_2077228
Cytokeratin 7	Mouse	Agilent	M7018	AB_2134589
E-Cadherin	Mouse	BD Biosciences	610182	AB_39581
EOMES	Rabbit	Abcam	ab23345	AB_778267
FOXA2	Goat	R&D Systems	AF2400	AB_2294104
FOXF1	Rabbit	ThermoFisher Scientific	PA5-50516	AB_2607993
GATA3	Goat	Abcam	ab199428	AB_2819013
GATA6	Goat	R&D Systems	AF1700	AB_2108901
GATA6	Rabbit	Cell Signaling Technology	5851	AB_10705521
GFP	Chicken	Abcam	ab13970	AB_300798
GFP	Rat	Nacalai USA	GF090R	AB_2314545
HAND1	Mouse	DSHB	PCRP-HAND1-2A9	AB_2618668
ISL1	Mouse	DSHB	PCRP-ISL1-1A9	AB_2618775
N-Cadherin	Mouse	Abcam	ab98952	AB_10696943
NANOG	Rabbit	Cell Signaling Technology	4903	AB_10559205
OCT3/4	Mouse	Santa Cruz Biotechnology	sc-5279	AB_628051
OTX2	Goat	R&D Systems	AF1979	AB_2157172
phosp-Smad1/5	Rabbit	Cell Signaling Technology	9516S	AB_491015
Smad2/3	Rabbit	Cell Signaling Technology	8685S	AB_10889933
SOX17	Goat	R&D Systems	AF1924	AB_355060
SOX2	Rat	ThermoFisher Scientific	14-9811-82	AB_11219471
TBX20	Mouse	R&D Systems	MAB8124	AB_2255728
VTCN1	Rabbit	Abcam	ab209242	AB_2801513

Table 2: List of primers used in this study

Primer	Sequence
qPCR_GATA6_Fwd	CTCAGTTCCTACGCTTCGCAT
qPCR_GATA6_Rev	GTCGAGGTCAGTGAACAGCA
qPCR_SOX17_Fwd	TTCGTGTGCAAGCCTGAGAT

bioRxiv preprint doi: https://doi.org/10.1101/2023.06.15.545082; this version posted June 15, 2023. The copyright holder for this preprint (which was not certified by peer review) is the author/funder, who has granted bioRxiv a license to display the preprint in perpetuity. It is made available under aCC-BY-NC-ND 4.0 International license.

qPCR_SOX17_Rev	TAATATACCGCGGAGCTGGC
qPCR_PDGFRA_Fwd	TGGCAGTACCCCATGTCTGAA
qPCR_PDGFRA_Rev	CCAAGACCGTCACAAAAAGGC
qPCR_GATA4_Fwd	CGACACCCCAATCTCGATATG
qPCR_GATA4_Rev	GTTGCACAGATAGTGACCCGT
qPCR_CER1_Fwd	ACAGTGCCCTTCAGCCAGACT
qPCR_CER1_Rev	ACAACTACTTTTTCACAGCCTTCGT
qPCR_COL4A1_Fwd	GGGATGCTGTTGAAAGGTGAA
qPCR_COL4A1_Rev	GGTGGTCCGGTAAATCCTGG
qPCR_SOX2_Fwd	GAGCTTTGCAGGAAGTTTGC
qPCR_SOX2_Rev	GCAAGAAGCCTCTCCTTGAA
qPCR_CD48_Fwd	AGGTTGGGATTCGTGTCTGG
qPCR_CD48_Rev	AGTTGTTTGTAGTTCTCAGGCAG
qPCR_GATA3_Fwd	GCCCCTCATTAAGCCCAAG
qPCR_GATA3_Rev	TTGTGGTGGTCTGACAGTTCG
qPCR_TFAP2C_Fwd	TGCACGATCAGACAGTCATTC
qPCR_TFAP2C_Rev	GTAGAGCTGAGGAGCGACAATC
qPCR_GATA2_Fwd	ACTGACGGAGAGCATGAAGAT
qPCR_GATA2_Rev	CCGGCACATAGGAGGGGTA
qPCR_TFAP2A_Fwd	AGGTCAATCTCCCTACACGAG
qPCR_TFAP2A_Rev	GGAGTAAGGATCTTGCGACTGG
qPCR_TACSTD2_Fwd	ACAACGATGGCCTCTACGAC
qPCR_TACSTD2_Rev	AGTTCACGCACCAGCACAC
qPCR_KRT19_Fwd	ACCTGGAGATGCAGATCGAA
qPCR_KRT19_Rev	AATCCACCTCCACACTGACC
qPCR_GABRP_Fwd	TTTCTCAGGCCCAATTTTCCT
qPCR_GABRP_Rev	GCTGTCGGAGGTATATGGTGG
qPCR_ISL1_Fwd	GCGGAGTGTAATCAGTATTTGGA
qPCR_ISL1_Rev	GCATTTGATCCCGTACAACCT
TFAP2C-AttB_Fwd	GGGGACAAGTTTGTACAAAAAAGCAGGCTTCACCATGTTGTGGA AAATAACCGATA
TFAP2C-AttB_Rev	GGGGACCACTTTGTACAAGAAAGCTGGGTCTTATTTCCTGTGTT TCTCCATT
SOX17-AttB_Fwd	GGGGACAAGTTTGTACAAAAAAGCAGGCTTCACCATGAGCAGCC CGGATGC
SOX17-AttB_Rev	GGGGACCACTTTGTACAAGAAAGCTGGGTCTCACACGTCAGGAT AGTTGCAG

622

bioRxiv preprint doi: https://doi.org/10.1101/2023.06.15.545082; this version posted June 15, 2023. The copyright holder for this preprint (which was not certified by peer review) is the author/funder, who has granted bioRxiv a license to display the preprint in perpetuity. It is made available under aCC-BY-NC-ND 4.0 International license.

Methods

Ethics Statement

Work with human embryonic stem cells (Shef6) was carried out with approval from the UK Human Stem Cell Bank Steering Committee under approval SCSC21-38 and adheres to the regulations of the UK Code of Practice for Use of Human Stem Cell Lines. Human embryo work was regulated by the Human Fertility and Embryology Authority (HFEA) and carried out under license R0193. Ethical approval was obtained from the Human Biology Research Ethics Committee at the University of Cambridge (reference HBREC.2021.26). IVF patients at CARE Fertility, Bourn Hall Fertility and Herts & Essex Fertility Clinics were provided project-specific information at the end of their treatment. All patients were offered counselling, received no financial benefit, and could withdraw their participation at any time until the embryo had been used for research. Embryos were not cultured beyond 14 d.p.f. or the first appearance of the primitive streak.

hESC culture

Shef6 human ESCs were cultured on Matrigel-coated plates in mTESR medium (05825, STEMCELL Technologies) at 37°C, 20% O2, 5% CO2. Plates were coated with 1.6% growth-factor reduced Matrigel (356230, BD Biosciences) dissolved in DMEM/F12 (21331-020, Life Technologies) for 1 hour at at 37°C. hESCs were passaged with TrypLE (12604013, ThermoFisher Scientific). For the first 24 hours after passaging, 10μM ROCK inhibitor Y-27632 (72304, STEMCELL Technologies) was added. Medium was changed every 24 hours. Cells were routinely tested for mycoplasma contamination by PCR (6601, Takara Bio). To convert primed hESCs to RSeT or PXGL culture conditions, cells were passaged to mitomycin-C inactivated CF-1 MEFs ($3x10^3$ cells/cm^2; GSC-6101G, Amsbio) in media consisting of DMEM/F12 with 20% Knockout Serum Replacement (10828010, ThermoFisher Scientific), 100μM β-mercaptoethanol (31350-010, Thermo Fisher Scientific), 1x GlutaMAX (35050061, Thermo Fisher Scientific), 1x

bioRxiv preprint doi: https://doi.org/10.1101/2023.06.15.545082; this version posted June 15, 2023. The copyright holder for this preprint (which was not certified by peer review) is the author/funder, who has granted bioRxiv a license to display the preprint in perpetuity. It is made available under aCC-BY-NC-ND 4.0 International license.

649 non-essential amino acids, 1x penicillin-streptomycin and 10ng/ml FGF2 (Department of
650 Biochemistry, University of Cambridge) and 10μM ROCK inhibitor Y-27632 (72304, STEMCELL
651 Technologies). For RSeT cells, media was switched to RSeT media after 24 hours (05978,
652 STEMCELL Technologies). Cells were maintained in RSeT and passaged as above every 4-5
653 days. For PXGL cells, conversion was performed as previously described[1]. Briefly, cells were
654 cultured in 5% O2, 7% CO2 and media was switched to chemical resetting media 1 (cRM-1)
655 consisting of N2B27 media supplemented with 1μM PD0325901 (University of Cambridge, Stem
656 Cell Institute), 10ng/mL human recombinant LIF (300-05, PeproTech), and 1mM Valproic Acid.
657 N2B27 contains 1:1 DMEM/F12 and Neurobasal A (10888-0222, Thermo Fisher Scientific)
658 supplemented with 0.5x B27 (10889-038, Thermo Fisher Scientific), 0.5x N2 (made in house),
659 100μM β-mercaptoethanol, 1x GlutaMAX and 1x penicillin-streptomycin. cRM-1 media was
660 changed every 48h for 4 days, after which media was changed to PXGL. PXGL media consists
661 of N2B27 supplemented with 1μM PD0325901, 10ng/mL human recombinant LIF, 2μM Gö6983
662 (2285, Tocris) and 2μM XAV939 (X3004, Merck). PXGL cells were passaged every 4-6 days
663 using TrypLE (12604013, Thermo Fisher Scientific) for 3 min. 10μM ROCK inhibitor Y-27632 and
664 1μL/cm^2 Geltrex (A1413201, Thermo Fisher Scientific) were added at passage for 24 hours. For
665 yolk sac-like cell or trophoblast differentiation, RSeT cells were passaged onto matrigel coated
666 IBIDI chamber slides. 24 hours later, media was switched to 'ACL' (100ng/ml Activin-A, Qk001,
667 QKINE, 3μM CHIR99021, 72052, STEMCELL Technologies, and 10ng/ml human LIF) for
668 hypoblast induction or 'PA' (1μM PD0325901 and 1μM A83-01, 72022, STEMCELL
669 Technologies) with or without 500nM lysophosphatidic acid – LPA (3854, Tocris).
670
671 *Generation of Inducible hESC lines*
672 To generate Piggyback plasmids, full length coding sequences were amplified from human cell
673 line cDNA with AttB overhangs using Phusion High-Fidelity DNA polymerase (M0530S, New

bioRxiv preprint doi: https://doi.org/10.1101/2023.06.15.545082; this version posted June 15, 2023. The copyright holder for this preprint (which was not certified by peer review) is the author/funder, who has granted bioRxiv a license to display the preprint in perpetuity. It is made available under aCC-BY-NC-ND 4.0 International license.

England BioLabs) according to manufacturer's instructions. Amplicons were introduced to pDONR221 entry plasmids using BP clonase (11789100, ThermoFisher Scientific), and subsequently to destination plasmids using LR clonase (11791020, ThermoFisherScientific) according to manufacturer's instructions. hESCs were electroporated with GATA6-3XFLAG-TetOn-Zeo (entry plasmid 72922, Addgene) and/or SOX17-TetOn-Hygro or GATA3-EGFP-TetO-Hygro (Gift from Dr. Mika Drukker) and/or TFAP2C-TetOn-G418 in addition to PB-CAG-rTTA3-Bsd or PB-CAG-rTTA3-Zeo and pBase plasmid expressing PiggyBac Transposase using the Neon transfection system with the following settings: 1200V, 2 ms, 2 pulses. Two days after transfection, antibiotics were applied at a ¼ dosage and increased to final concentrations of 100µg/mL zeocin (ant-zn-1, Invitrogen), 20µg/mL blasticidin (A113903, ThermoFisher Scientific), 50µg/mL G418 (10131035, ThermoFisher Scientific) or 50µg/mL HygromycinB (10687010, ThermoFisher Scientific). Clones were generated by manually picking single colonies under a dissecting microscope. Transgene activation was triggered by addition of 1µg/mL doxycycline hyclate (D9891, Sigma). Note that AP2γ-inducible cells failed to reset in PXGL naïve conditions.

qRT-PCR Analysis

Cell pellets were harvested and RNA was extracted using the Qiagen RNeasy kit following manufacturer's instructions. Reverse Transcriptase reaction was performed with 1µg RNA with random primers (C1181, Promega), dNTPs (N0447S, New England BioLabs), RNAse inhibitor (M0314L, New England Biolabs, and M-MuLV reverse transcriptase (M0253L, New England Biolabs). RT-qPCR was performed using Power SYBR Green PCR Master Mix (4368708, ThermoFisher Scientific) on a Step One Plus Real-Time PCR machine (Applied Biosystems). The following program was used: 10 minutes at 95ºC followed by 40 cycles of 15s at 95ºC and 1 minute at 60ºC. Single melt curves were observed for all primers used in this study.

Generation of Inducible Human Embryoids

bioRxiv preprint doi: https://doi.org/10.1101/2023.06.15.545082; this version posted June 15, 2023. The copyright holder for this preprint (which was not certified by peer review) is the author/funder, who has granted bioRxiv a license to display the preprint in perpetuity. It is made available under aCC-BY-NC-ND 4.0 International license.

To generate the three-dimensional stem cell-derived model of the post-implantation embryo, RSeT cells between 2 and 6 passages post-conversion to RSeT media were passaged as normal; the following day (Day -3) the media for extraembryonic-like cells (induced GATA6, induced GATA6-SOX17 or induced GATA3-AP2γ) was changed to N2B27 with 5% Knockout Serum Replacement and 1µg/mL DOX. This media was refreshed every 24 hours for 3 days. On day 0 (the day of aggregation), an Aggrewell dish (34415, STEMCELL Technologies) was prepared by pre-coating with anti-adherance solution (07010, STEMCELL Technologies) and centrifuging at 2000g for 5 minutes. Wells were washed twice with PBS prior to the addition of experiment media. This media consists of N2B27 with 5% knockout serum replacement, 1µg/mL doxycycline and 10µM Y-27632. Induced cells and wild type ESCs were enzymatically dissociated 1 hour after addition of 10µM Y-27632 to wells containing cells for inducible human embryoid generation. Dissociated cells were pelleted and resuspended in experiment media and placed in gelatin-coated wells for MEF depletion. After 15-30 minutes cells were counted, mixed, and plated into an Aggrewell dish with a final calculation of 8 wildtype-ESC, 8 hypoblast-like and 16 trophoblast-like cells plated per microwell in the Aggrewell. On day 1, the media was subjected to two two-third changes of N2B27 with 5% knockout serum replacement and 1µg/mL doxycycline. On day 2, Aggrewells were subjected to a half change with hIVC1 media with 1.25 µg/mL hIGF1 (78022.1 STEMCELL Technologies) and 1µg/mL doxycycline. hIVC1 media consists of Advanced DMEM/F12 (12634-010 ThermoFisher Scientific) supplemented with 20% inactivated FBS (10270106, ThermoFisher Scientific), 1x Glutamax, 1X NEAA, 1x Essential AA, 1x ITS-X, 25U/mL Pen/Strep, 1.8mM Glucose (G8644, Sigma-Aldrich), 0.22% sodium lactate (L7900, Sigma-Aldrich), 8nM β-estradiol (50-28-2, Tocris) and 200ng/mL progesterone (P0130, Sigma-Aldrich). This media is used in half changes each day from day 3. On day 4, aggregates were manually picked using a mouth pipette under a dissecting microscope into individual wells of ultra-low attachment 96 well plates (CLS7007, Corning) in hIVC1 media with IGF1 and doxycycline as above for subsequent culture.

bioRxiv preprint doi: https://doi.org/10.1101/2023.06.15.545082; this version posted June 15, 2023. The copyright holder for this preprint (which was not certified by peer review) is the author/funder, who has granted bioRxiv a license to display the preprint in perpetuity. It is made available under aCC-BY-NC-ND 4.0 International license.

726

727 *Immunostaining and image analysis*

728 Samples were washed with phosphate-buffered saline (PBS) and fixed in 4% Paraformaldehyde
729 (PFA; 1710, Electron Microscopy Sciences) at room temperature for 20 minutes. Samples were
730 washed 3 times with PBS + 0.1% (vol/vol) Tween-20 (PBST) and incubated with 0.3% (vol/vol)
731 Triton X-100 (T8787, Sigma Aldrich) + 0.1mM glycine (BP381-1, Thermofisher Scientific) in PBS
732 at room temperature for 30 minutes. Samples were blocked in blocking buffer (PBST with 5%
733 (w/vol) BSA, A9418, Sigma), then incubated with primary antibodies diluted in blocking buffer
734 overnight at 4ºC. See table 1 for a list of primary antibodies. Samples were washed three times
735 in PBST and incubated with fluorescently conjugated AlexaFlour secondary antibodies
736 (Thermofisher Scientific, 1:500) and DAPI (D3571, ThermoFisher Scientific, 1μg/ml) diluted in
737 blocking buffer for 2 hours at room temperature. For pSMAD1.5 quantification, OCT4-positive or
738 GATA6-positive nuclei were isolated and the fluorescent intensity of pSMAD1.5 was quantified.
739 For SMAD2.3 quantification, OCT4-positive or GATA6-positive (excluding the outermost GFP+
740 cell layer) nuclei fluorescence intensity was quantified, as well as cytoplasmic fluorescence
741 intensity. Data is presented as the ratio of nuclear:cytoplasmic fluorescence intensity.
742 Immunofluorescence images were analyzed using FIJI.

743

744 *Human Embryo Thawing and Culture*

745 Human embryos were thawed and cultured as described previously[2,3]. Briefly, cryopreserved
746 human blastocysts (5 or 6 d.p.f.) were thawed using the Kitazato thaw kit (VT8202-2, Hunter
747 Scientific) according to the manufacturer's instructions. The day prior to thawing, TS solution was
748 placed at 37°C overnight. The next day, IVF straws were submerged in 1mL pre-warmed TS for
749 1 min. Embryos were then transferred to DS for 3 min, WS1 for 5 min, and WS2 for 1 min. These
750 steps were performed in reproplates (REPROPLATE, Hunter Scientific) using a STRIPPER
751 micropipette (Origio). Embryos were incubated at 37°C and 5% CO2 in normoxia and in pre-

bioRxiv preprint doi: https://doi.org/10.1101/2023.06.15.545082; this version posted June 15, 2023. The copyright holder for this preprint (which was not certified by peer review) is the author/funder, who has granted bioRxiv a license to display the preprint in perpetuity. It is made available under aCC-BY-NC-ND 4.0 International license.

equilibrated human IVC1 supplemented with 50ng/mL Insulin Growth Factor-1 (IGF1) (78078, STEMCELL Technologies) under mineral oil for 1-4h to allow for recovery. Following thaw, blastocysts were briefly treated with acidic Tyrode's solution (T1788, Sigma) to remove the zona pellucida and placed in pre-equilibrated human IVC1 in 8 well µ-slide tissue culture plates (80826, Ibidi) in approximately 400 µL volume per embryo per well. Half media changes were done every 24 hours.

Statistics

Statistical analyses were performed using Graphpad Prism 9. Sample sizes were not predetermined, and the authors were not blinded to conditions. All experiments were performed independently at least twice. Within plots, all data is presented as mean ± SEM.

Collection, Generation and Sequencing of single-nuclei ATAC/RNA 10x Libraries

To collect post-implantation embryo models for single-cell sequencing, correctly organized embryoids at day 4, 6 and 8 were picked visually and washed through PBS twice in a 4-well dish before transfer to TrypLE. Samples were agitated by pipetting every 5 minutes for 10-20 minutes until dissociated. Enzymatic activity was inactivated through addition of 20% FBS in PBS at 2x volume. Cells were collected in a falcon tube, pelleted, and resuspended in freeze buffer consisting of 50 mM Tris at pH 8.0 (15-567-027, Fisher Scientific), 25% glycerol (G5516, Sigma-Aldrich), 5 mM Mg(OAc)2 (63052, Sigma-Aldrich), 0.1mM EDTA (15575020, ThermoFisher Scientific), 5mM DTT (R0861, ThermoFisher Scientific), 1x protease inhibitor cocktail (P8340, Sigma-Aldrich), 1:2500 dilution of superasin (AM2694, Invitrogen). For cell lines, 10,000 cells were counted, pelleted, and resuspended in the freeze media above before slowfreezing at -80ºC.

For nuclei isolation and library construction, low input nuclei isolation protocol from 10x Genomics was performed. Briefly, frozen cell pellets were thawed in a 37°C water bath for 30 seconds,

bioRxiv preprint doi: https://doi.org/10.1101/2023.06.15.545082; this version posted June 15, 2023. The copyright holder for this preprint (which was not certified by peer review) is the author/funder, who has granted bioRxiv a license to display the preprint in perpetuity. It is made available under aCC-BY-NC-ND 4.0 International license.

778 centrifuged (500g for 5 minutes at 4°C) to pellet the cells then the supernatant were aspirated.
779 The cell pellets were washed with 200 µl 1x PBS with 0.04% BSA twice, centrifuged, and
780 supernatant was aspirated between washes. Subsequently, chilled lysis buffer (45 µl per sample)
781 was added to the washed cell pellet and placed on ice for 3 minutes, then wash buffer (50 µl per
782 sample) was added. Washed isolated nuclei were resuspended in a diluted nuclei buffer. In this
783 study, the isolated nuclei were resuspended in 5 µl of diluted nuclei buffer and were directly added
784 to the transposition reaction. In all following steps, 10x Genomics' Single Cell Multiome ATAC
785 and Gene expression protocol were followed according to manufacturer's specifications and
786 guidelines. The final libraries were loaded on the NextSeq 2000 using P2 100 cycle kit at 650 pM
787 loading concentration with paired end sequencing following the recommended sequencing reads
788 from 10x Genomics (28/10/10/90 cycles for gene expression libraries and 50/8/24/49 cycles for
789 ATAC libraries).
790
791 *Single Cell Sequencing Analysis*
792 Processing and Quality Control
793 Raw reads were analyzed using the CellRangerARC pipeline to generate ATAC and RNA fastq
794 files for each sample, and then to align genomic and transcriptomic reads. Matrices were then
795 read into Seurat[4] and Signac[5] using the Read10X_h5 command. For ATAC-seq data, peaks from
796 standard chromosomes were used and peaks were additionally called using macs2 to add an
797 additional Signac assay. Cells with >500 RNA UMI counts, <20% mitochondrial reads, >500
798 ATAC reads, TSS enrichment >1 and were called as singlets using scDblFinder[6] were retained
799 for downstream analysis. For UMAP projections, SCTransform was used for RNA counts with
800 percent mitochondrial counts and cell cycle scores regressed. PCA and LSI graphs were used to
801 generate a weighted nearest neighbor (wnn) embedding which accounts for both modalities.
802 chromVAR[7] was run to calculate motif accessibility score on the peaks assay.
803

bioRxiv preprint doi: https://doi.org/10.1101/2023.06.15.545082; this version posted June 15, 2023. The copyright holder for this preprint (which was not certified by peer review) is the author/funder, who has granted bioRxiv a license to display the preprint in perpetuity. It is made available under aCC-BY-NC-ND 4.0 International license.

Comparisons to Published Datasets

scmap[8] was used to project cell labels from other single cell datasets onto post-implantation embryo model transcriptional data. All reference data used was publicly available with published cell type annotations. Cynomolgus monkey gene names were converted to hgnc gene symbols using biomaRt. For data generated with smart-seq2 or other non-UMI-based single cell sequencing methods, the scmapCluster method was used with a similarity threshold of 0.5. For UMI-based methods the scmapCell followed by scmapCell2Cluster method was used with w=2. Upon cell type assignment and processing for the cell lines sequenced, a logistic regression framework was applied to project cell line data onto published single cell data and to project published cluster annotations onto post-implantation embryo model clusters, resulting in a quantitative measure of predicted similarities[9]. Here, only differentially expressed genes (produced using Seurat's FindAllMarkers function on course cell assignments (which collapsed amnion and mesodermal clusters) were used.

Multivelo RNA/Chromatin Velocity

We applied a recently published method for velocity calculations that accounts for both single cell ATAC and RNA data[10]. Multivelo was run on all cells which passed the QC and processing described above. Analysis was based on available vignettes with 1000 highly variable genes and the 'grid' method.

CellPhoneDB Analysis

CellPhoneDB 2.0 was used with default settings to assess potential tissue signaling crosstalk[11]. Course cell assignments which collapsed separated amnion (AM-1, AM-2, AM-3) and mesoderm (MESO-1, MESO-2) clusters was used for simplicity. Selected significant interactions were plotted as dot plots.

bioRxiv preprint doi: https://doi.org/10.1101/2023.06.15.545082; this version posted June 15, 2023. The copyright holder for this preprint (which was not certified by peer review) is the author/funder, who has granted bioRxiv a license to display the preprint in perpetuity. It is made available under aCC-BY-NC-ND 4.0 International license.

Reanalysis of human *in vitro* cultured embryo datasets

Previously published data from Yan et al., Blakely et al., Petropolous et al., Zhou et al., and Xiang et al., were realigned to the hg38 human genome using kallisto or kb-bustools[12,13]. Datasets which were not sequenced with UMI-based technologies were normalized using quminorm to quasi-umis[14]. Using SCTransform-based integration, datasets were combined to generate a single-cell RNA-seq dataset of human embryos spanning zygote to day 14 post-fertilization[2,15-19]. Cells were clustered and identities assigned based on previous annotations and canonical marker expression. SCENIC was used with default settings in R, and the AUC-regulon table used to generate a new assay in the Seurat object. Using this assay, the epiblast, hypoblast and trophoblast lineages were then compared using Seurat's FindMarkers function to identify predicted differentially active regulons. These factors were then plotted in relation to each other in Cytoscape.

Data Availability Statement

Data generated in this study is available under Gene Expression Omnibus accession code GSE218314. For the purpose of revew this dataset can be accessed with the token ijkhciquzhubbqt.

Previously published data is publicly available:

Human data

Molè et al., 2021: ArrayExpress E-MTAB-8060

Xiang et al., 2020: Gene Expression Omnibus GSE136447

Zhou et al., 2019: Gene Expression Omnibus GSE109555

Petropoulos et al., 2016: ArrayExpress E-MTAB-3929

Blakely et al., 2015: Gene Expression Omnibus GSE66507

Yan et al., 2013: Gene Expression Omnibus GSE36552

bioRxiv preprint doi: https://doi.org/10.1101/2023.06.15.545082; this version posted June 15, 2023. The copyright holder for this preprint (which was not certified by peer review) is the author/funder, who has granted bioRxiv a license to display the preprint in perpetuity. It is made available under aCC-BY-NC-ND 4.0 International license.

Cynomolgus Monkey

Yang et al., 2021: Gene Expression Omnibus GSE148683

Ma et al., 2019: Gene Expression Omnibus GSE130114

Nakamura et al., 2016: Gene Expression Omnibus GSE74767

Code Availability Statement

Code to used to analyze these data is available at https://github.com/bweatherbee/human_model

(to be made public upon publication)

Methods References

1 Bredenkamp, N. *et al.* Wnt Inhibition Facilitates RNA-Mediated Reprogramming of Human Somatic Cells to Naive Pluripotency. *Stem cell reports* **13**, 1083-1098 (2019). https://doi.org:10.1016/j.stemcr.2019.10.009

2 Molè, M. A. *et al.* A single cell characterisation of human embryogenesis identifies pluripotency transitions and putative anterior hypoblast centre. *Nature Communications* **12** (2021). https://doi.org:10.1038/s41467-021-23758-w

3 Shahbazi, M. N. *et al.* Self-organization of the human embryo in the absence of maternal tissues. *Nature Cell Biology* **18**, 700-708 (2016). https://doi.org:10.1038/ncb3347

4 Stuart, T. *et al.* Comprehensive Integration of Single-Cell Data. *Cell* **177**, 1888-1902.e1821 (2019). https://doi.org:10.1016/j.cell.2019.05.031

5 Stuart, T., Srivastava, A., Madad, S., Lareau, C. A. & Satija, R. Single-cell chromatin state analysis with Signac. *Nat Methods* **18**, 1333-1341 (2021). https://doi.org:10.1038/s41592-021-01282-5

6 Germain, P. L., Lun, A., Garcia Meixide, C., Macnair, W. & Robinson, M. D. Doublet identification in single-cell sequencing data using scDblFinder. *F1000Res* **10**, 979 (2021). https://doi.org:10.12688/f1000research.73600.2

7 Schep, A. N., Wu, B., Buenrostro, J. D. & Greenleaf, W. J. chromVAR: inferring transcription-factor-associated accessibility from single-cell epigenomic data. *Nat Methods* **14**, 975-978 (2017). https://doi.org:10.1038/nmeth.4401

8 Kiselev, V. Y., Yiu, A. & Hemberg, M. scmap: projection of single-cell RNA-seq data across data sets. *Nat Methods* **15**, 359-362 (2018). https://doi.org:10.1038/nmeth.4644

9 Young, M. D. *et al.* Single-cell transcriptomes from human kidneys reveal the cellular identity of renal tumors. *Science* **361**, 594-599 (2018). https://doi.org:10.1126/science.aat1699

10 Li, C., Virgilio, M. C., Collins, K. L. & Welch, J. D. Multi-omic single-cell velocity models epigenome-transcriptome interactions and improves cell fate prediction. *Nat Biotechnol* (2022). https://doi.org:10.1038/s41587-022-01476-y

11 Efremova, M., Vento-Tormo, M., Teichmann, S. A. & Vento-Tormo, R. CellPhoneDB: inferring cell–cell communication from combined expression of multi-subunit ligand–receptor complexes. *Nature Protocols* **15**, 1484-1506 (2020). https://doi.org:10.1038/s41596-020-0292-x

12 Bray, N. L., Pimentel, H., Melsted, P. & Pachter, L. Near-optimal probabilistic RNA-seq quantification. *Nature Biotechnology* **34**, 525-527 (2016). https://doi.org:10.1038/nbt.3519

bioRxiv preprint doi: https://doi.org/10.1101/2023.06.15.545082; this version posted June 15, 2023. The copyright holder for this preprint (which was not certified by peer review) is the author/funder, who has granted bioRxiv a license to display the preprint in perpetuity. It is made available under aCC-BY-NC-ND 4.0 International license.

13 Melsted, P. *et al.* Modular, efficient and constant-memory single-cell RNA-seq preprocessing. *Nature Biotechnology* **39**, 813-818 (2021). https://doi.org:10.1038/s41587-021-00870-2

14 Townes, F. W. & Irizarry, R. A. Quantile normalization of single-cell RNA-seq read counts without unique molecular identifiers. *Genome Biology* **21** (2020). https://doi.org:10.1186/s13059-020-02078-0

15 Yan, L. *et al.* Single-cell RNA-Seq profiling of human preimplantation embryos and embryonic stem cells. *Nature Structural and Molecular Biology* **20**, 1131-1139 (2013). https://doi.org:10.1038/nsmb.2660

16 Blakeley, P. *et al.* Defining the three cell lineages of the human blastocyst by single-cell RNA-seq. *Development (Cambridge)* **142**, 3613-3613 (2015). https://doi.org:10.1242/dev.131235

17 Petropoulos, S. *et al.* Single-Cell RNA-Seq Reveals Lineage and X Chromosome Dynamics in Human Preimplantation Embryos. *Cell* **165**, 1012-1026 (2016). https://doi.org:10.1016/j.cell.2016.03.023

18 Zhou, F. *et al.* Reconstituting the transcriptome and DNA methylome landscapes of human implantation. *Nature* **572**, 660-664 (2019). https://doi.org:10.1038/s41586-019-1500-0

19 Xiang, L. *et al.* A developmental landscape of 3D-cultured human pre-gastrulation embryos. *Nature* **577**, 537-542 (2020). https://doi.org:10.1038/s41586-019-1875-y

Acknowledgements

The authors are grateful to CARE Fertility, Herts and Essex Fertility Centre, Bourn Hall Fertility Clinic and King's Fertility Clinic for their collaboration in donation of supernumerary human embryos. The authors thank all members of the M.Z-G and Boroviak labs, Gianluca Amadei for thoughtful comments and Marta Shahbazi and David Glover for feedback on the manuscript. This work is supported by Wellcome Trust, Open Atlas and NOMIS award grants to M.Z-G, Allen Discovery Center for Cell Lineage Tracing grants to J.S. and M.Z-G., in addition to individual funding from the Gates Cambridge Trust (to B.A.T.W.) and Leverhulme Trust Early Career Fellowship (to C.W.G.). J.S. is an investigator of the Howard Hughes Medical Institute.

Author Contributions

B.A.T.W. and C.W.G. designed, carried out, and analyzed experiments. B.A.T.W., C.W.G. and L.K.I-S. performed human embryo work. N.H. and R.M.D. prepared 10x multiome libraries and performed RNA and ATAC sequencing supervised by J.S.. B.A.T.W. analyzed single-cell sequencing data. C.W.G. and B.A.T.W. wrote the manuscript with input from all co-authors. M.Z-G conceived and supervised the project.

bioRxiv preprint doi: https://doi.org/10.1101/2023.06.15.545082; this version posted June 15, 2023. The copyright holder for this preprint (which was not certified by peer review) is the author/funder, who has granted bioRxiv a license to display the preprint in perpetuity. It is made available under aCC-BY-NC-ND 4.0 International license.

Declarations of Interests

M.Z-G, B.A.T.W and C.W.G are inventors on a patent titled ‘Stem Cell Derived-Model of the Human Embryo.”

bioRxiv preprint doi: https://doi.org/10.1101/2023.06.15.545082; this version posted June 15, 2023. The copyright holder for this preprint (which was not certified by peer review) is the author/funder, who has granted bioRxiv a license to display the preprint in perpetuity. It is made available under aCC-BY-NC-ND 4.0 International license.

Extended Data

Extended Figure 1

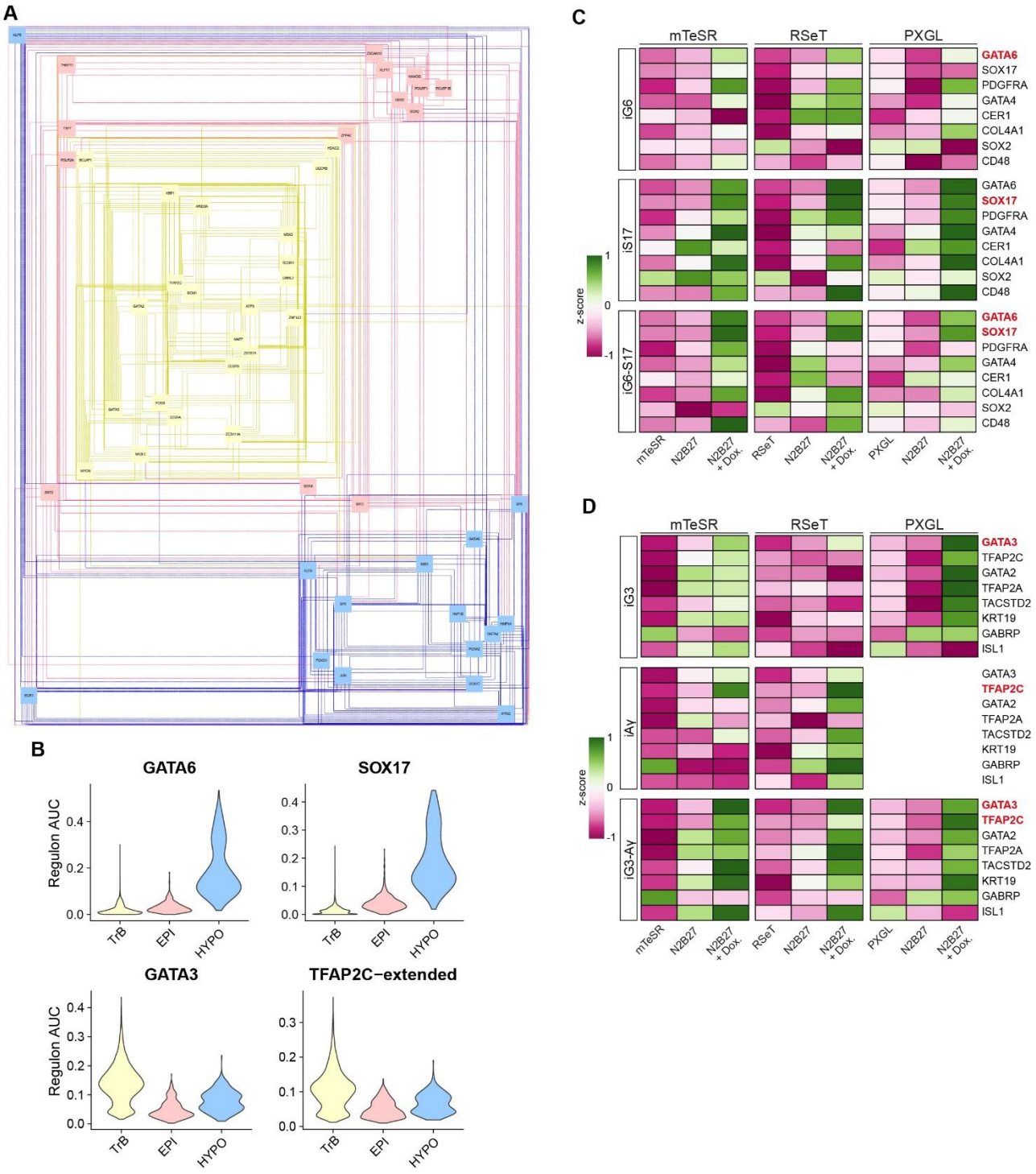

Extended Figure 1 (related to Fig 1) – Sequencing analysis and gene regulatory network generation to guide transgene selection.

(A) Inferred epiblast, hypoblast and trophoblast gene regulatory network generated by SCENIC during peri-implantation human embryo development. See methods for details on datasets and processing. (B) Regulon activity scored by SCENIC for hypoblast markers GATA6, SOX17 and TrB markers GATA3 and TFAP2C. (C) qRT-PCR analysis after 3 days of doxycycline-induction of induced GATA6 (iG6), induced SOX17 (iS17) or induced GATA6-SOX17 (iG6-S17)

bioRxiv preprint doi: https://doi.org/10.1101/2023.06.15.545082; this version posted June 15, 2023. The copyright holder for this preprint (which was not certified by peer review) is the author/funder, who has granted bioRxiv a license to display the preprint in perpetuity. It is made available under aCC-BY-NC-ND 4.0 International license.

942 singly and together from three pluripotent states. N=3 technical replicates from 3 biological replicates. (D) qRT-PCR
943 analysis after 3 days of DOX-induction of induced GATA3 (iG3), induced AP2γ (iAγ) or induced GATA3-AP2γ (iG3-Aγ)
944 from multiple pluripotent starting states. N=3 technical replicates for 3 biological replicates. Note, for (C) and (D) the
945 induced transgenes are marked in red.
946

bioRxiv preprint doi: https://doi.org/10.1101/2023.06.15.545082; this version posted June 15, 2023. The copyright holder for this preprint (which was not certified by peer review) is the author/funder, who has granted bioRxiv a license to display the preprint in perpetuity. It is made available under aCC-BY-NC-ND 4.0 International license.

Extended Figure 2

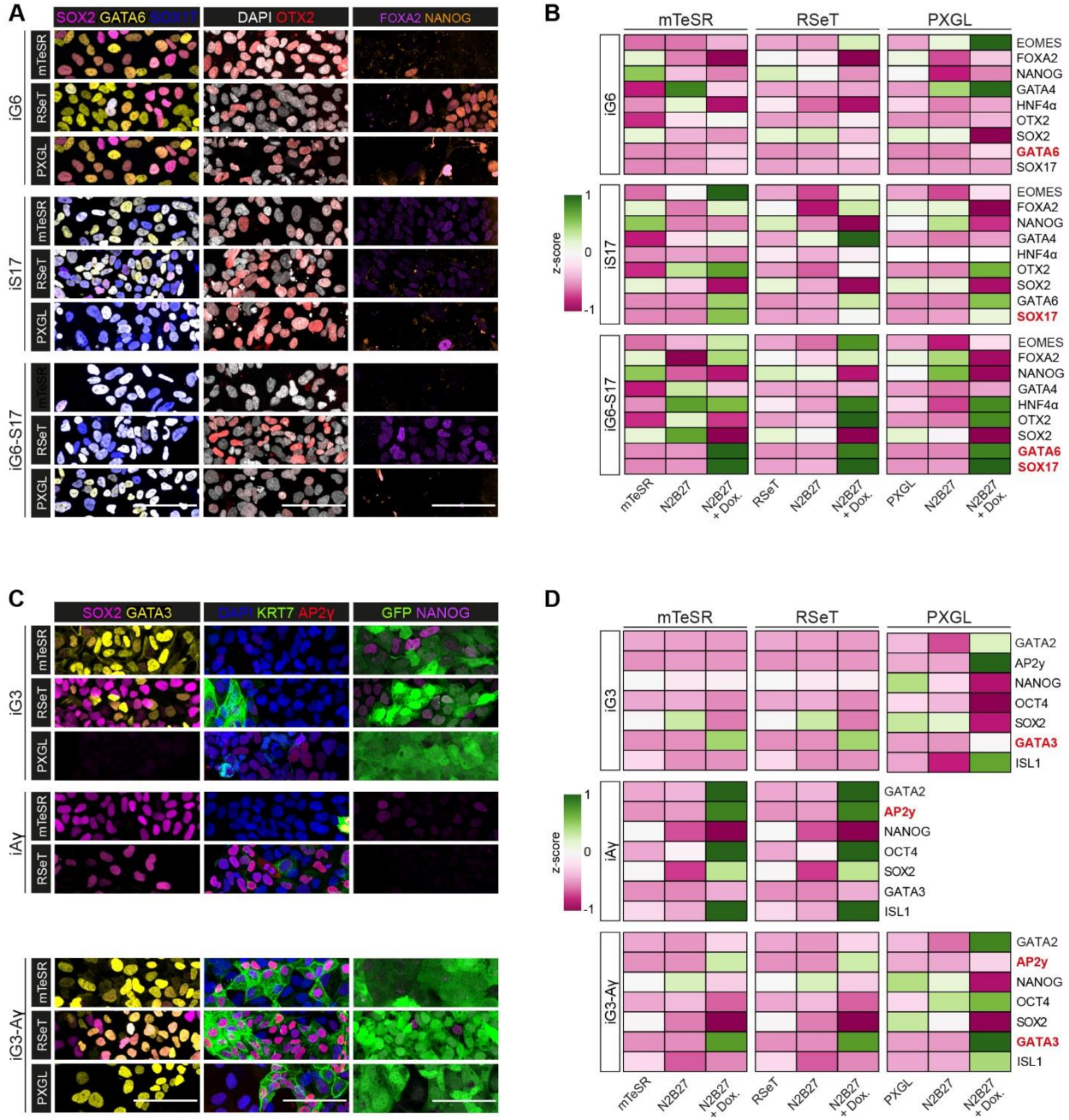

Extended Figure 2 (related to Fig 1) – Immunofluorescence analysis of cardinal marker genes of hypoblast and trophoblast after doxycycline induction across pluripotent states.
(A) Immunofluorescence analysis of inducible GATA6 (iG6), inducible SOX17 (S17) or inducible GATA6-SOX17 (iG6-S17) cells after 3 days induction from multiple pluripotent states. (B) Quantification of A. (C) Immunofluorescence analysis of inducible GATA3 (iG3), inducible AP2γ (iAγ) or inducible GATA3-AP2γ (iG3-Aγ) after 3 days induction from multiple pluripotent states. Note, for (B) and (D) the induced transgenes are marked in red. For all, N=3 technical replicates from 2 independent experiments.

bioRxiv preprint doi: https://doi.org/10.1101/2023.06.15.545082; this version posted June 15, 2023. The copyright holder for this preprint (which was not certified by peer review) is the author/funder, who has granted bioRxiv a license to display the preprint in perpetuity. It is made available under aCC-BY-NC-ND 4.0 International license.

Extended Figure 3

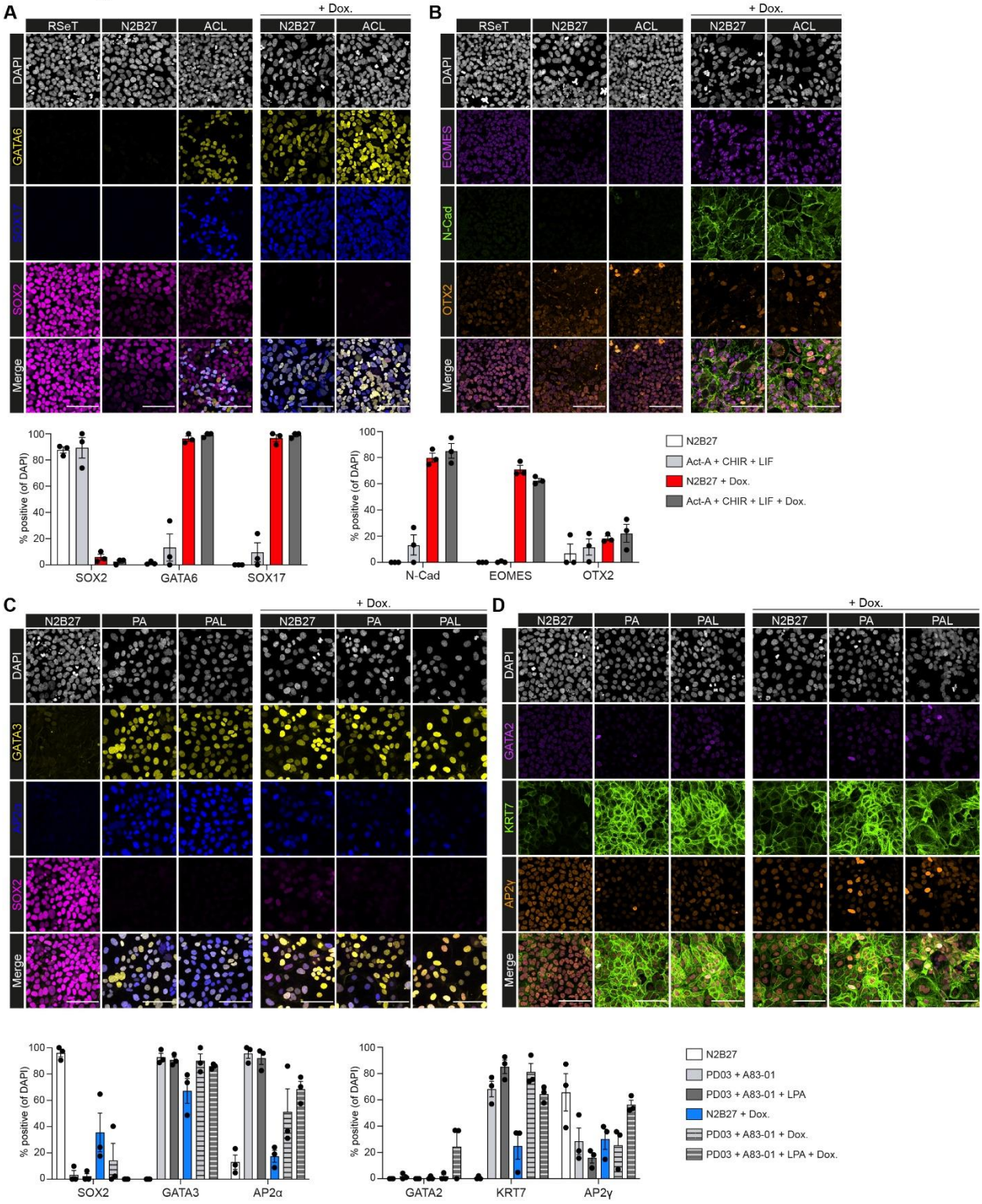

Extended Figure 3 (related to Fig 1) – Comparison of TF-mediated induction with published directed differentiation methods.

(A) Comparison and quantification of GATA6, SOX17 and SOX2 after yolk sac-like cell (Activin-A, CHIR99021 and LIF) directed differentiation, doxycycline-mediated induction in inducible GATA6-SOX17 cells or both. Cells were

bioRxiv preprint doi: https://doi.org/10.1101/2023.06.15.545082; this version posted June 15, 2023. The copyright holder for this preprint (which was not certified by peer review) is the author/funder, who has granted bioRxiv a license to display the preprint in perpetuity. It is made available under aCC-BY-NC-ND 4.0 International license.

961 differentiated from RSeT conditions. (B) Comparison and quantification of EOMES, N-Cadherin and OTX2 after yolk-
962 sac like cell (Activin-A, CHIR99021 and LIF) directed differentiation, doxycycline-mediated induction in inducible
963 GATA6-SOX17 cells or both. N=2994 cells. (C) Comparison and quantification of GATA3, AP2α and SOX2 after PA
964 (PD0325901 and A83-01) or PAL (PD0325901, A83-01 and LPA) directed differentiation, doxycycline-mediated
965 induction in inducible GATA3-AP2γ cells or both. (D) Comparison and quantification of GATA2, KRT7 and AP2γ after
966 PA (PD0325901 and A83-01) or PAL (PD0325901, A83-01 and LPA) directed differentiation, doxycycline-mediated
967 induction in inducible GATA3-AP2γ RSeT cells or both. N=2368 cells. Differentiation was carried out on hESC in RSeT
968 conditions.
969

bioRxiv preprint doi: https://doi.org/10.1101/2023.06.15.545082; this version posted June 15, 2023. The copyright holder for this preprint (which was not certified by peer review) is the author/funder, who has granted bioRxiv a license to display the preprint in perpetuity. It is made available under aCC-BY-NC-ND 4.0 International license.

Extended Figure 4

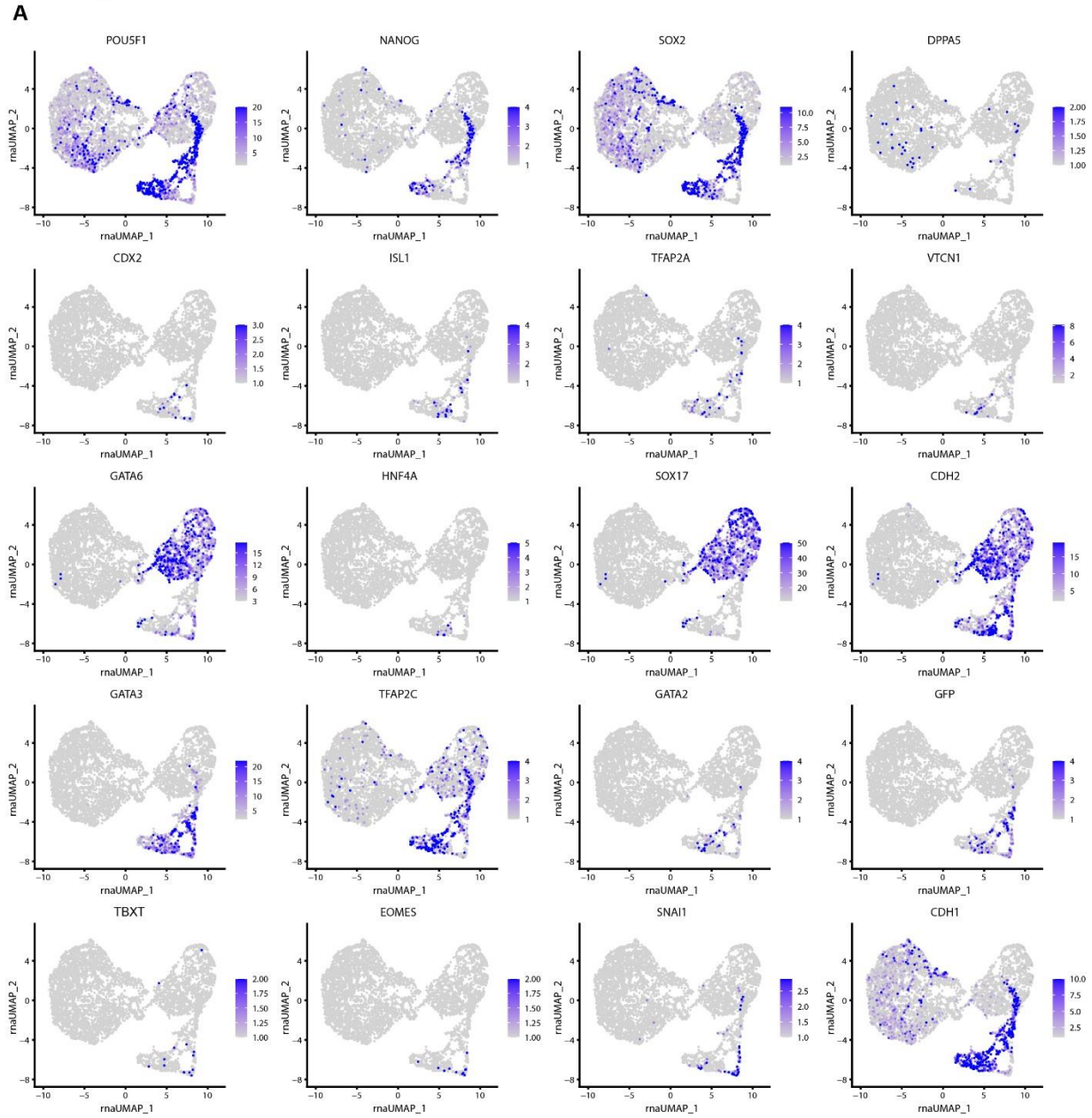

Extended Figure 4 (related to Fig 1) – Expression of cardinal marker genes after three days of induction from RSeT cells.

(A) UMAP projections of selected genes after 3 days of doxycycline-induction from sequencing of wildtype, inducible GATA6-SOX17 and inducible GATA3-AP2γ RSeT hESC populations. Induction was carried out from hESC in RSeT conditions.

bioRxiv preprint doi: https://doi.org/10.1101/2023.06.15.545082; this version posted June 15, 2023. The copyright holder for this preprint (which was not certified by peer review) is the author/funder, who has granted bioRxiv a license to display the preprint in perpetuity. It is made available under aCC-BY-NC-ND 4.0 International license.

Extended Figure 5

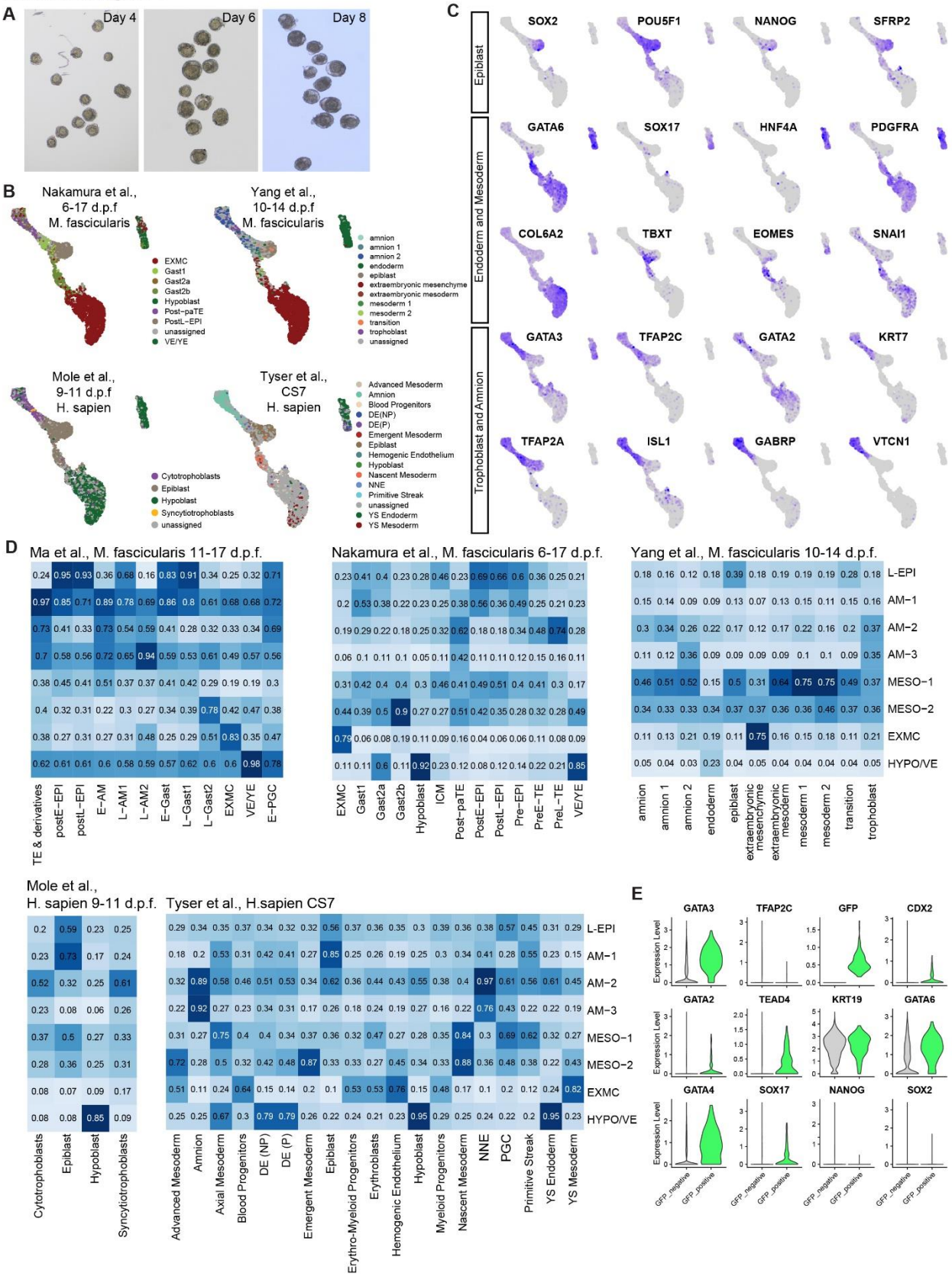

bioRxiv preprint doi: https://doi.org/10.1101/2023.06.15.545082; this version posted June 15, 2023. The copyright holder for this preprint (which was not certified by peer review) is the author/funder, who has granted bioRxiv a license to display the preprint in perpetuity. It is made available under aCC-BY-NC-ND 4.0 International license.

Extended Figure 5 (related to Fig 3) – Post-implantation human model cluster identification and comparison to human and cynomolgus monkey datasets.

(A) Brightfield image of inducible human embryoids selected at days 4, 6 and 8 for sequencing (n=12 at each stage). Note the presence of an inner domain surrounded by two concentric domains. (B) Cardinal marker gene expression for Epiblast, Endoderm and Mesoderm, and Trophoblast and Amnion within the stem cell derived model. (C) scmap projection of inducible human embryoid cells onto cynomolgus macaque (*M. fasicularis*) and human datasets (*H. sapien*) spanning peri-implantation to gastrulation stages. (D) Logistic regression analysis projecting annotated clusters from cynomolgus macaque (*M. fasicularis*) and human datasets (*H. sapien*) spanning peri-implantation to gastrulation stages onto post-implantation human embryo model clusters. Cynomolgus data from Ma et al., 2019, Nakamura et al., 2016, Yang et al., 2021; Human data from Molè et al., 2021 and Tyser et al., 2021. (E) Violin plots of gene expression in GFP-negative versus GFP-positive cells derived from induced GATA3-AP2γ cells from inducible human embryoid sequencing dataset.

bioRxiv preprint doi: https://doi.org/10.1101/2023.06.15.545082; this version posted June 15, 2023. The copyright holder for this preprint (which was not certified by peer review) is the author/funder, who has granted bioRxiv a license to display the preprint in perpetuity. It is made available under aCC-BY-NC-ND 4.0 International license.

Extended Figure 6

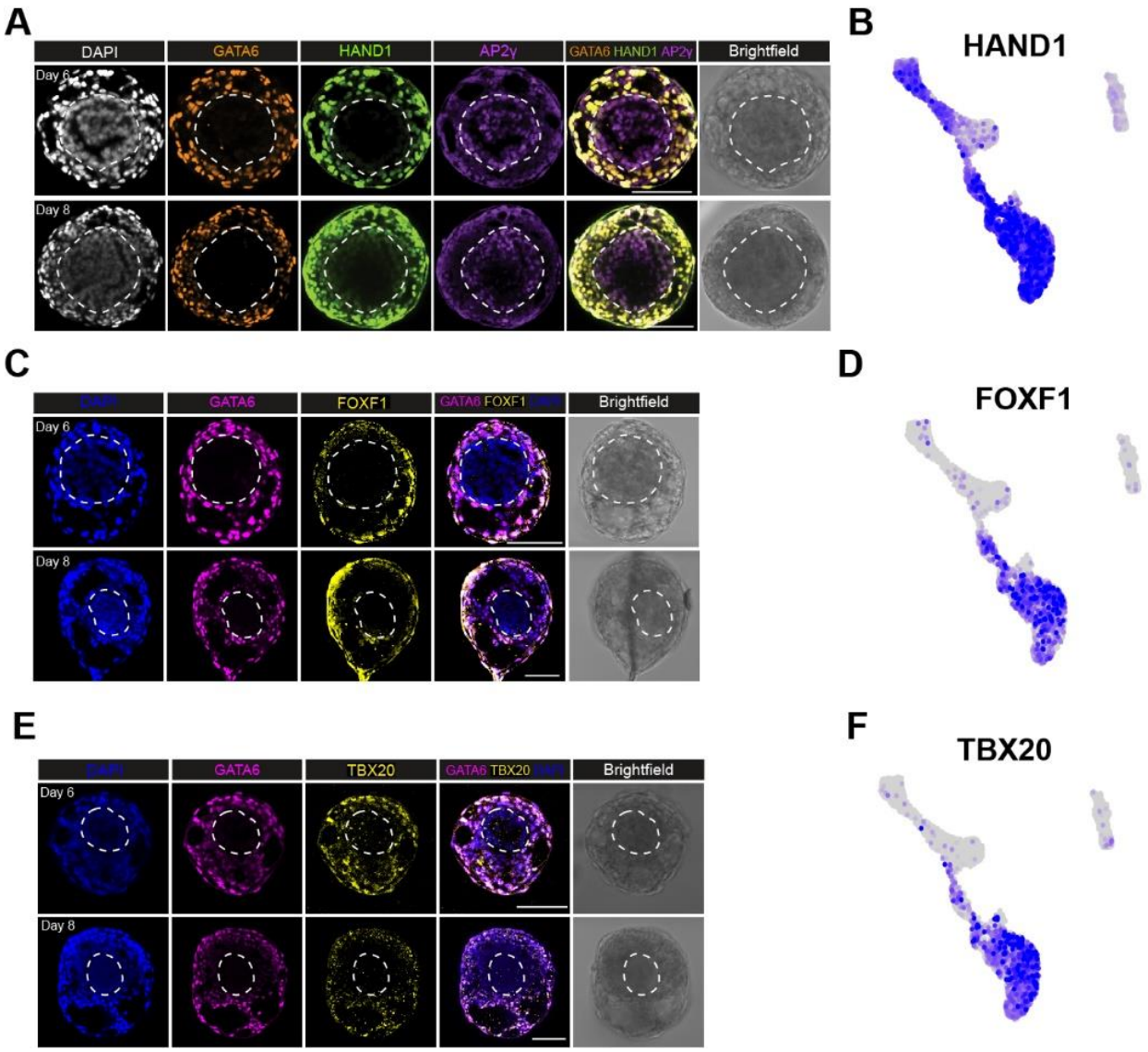

Extended Figure 6 (related to Fig 3) – Upregulation of HAND1 in extraembryonic mesenchyme and amnion trajectories.

(A) Immunofluorescence of HAND1 demonstrating expression in GATA6-positive cells (putative extraembryonic mesenchyme) and upregulation between days 4 and 6 in putative amnion (AP2γ-positive). (B) Expression of *HAND1* in the inducible human embryoid single cell sequencing dataset. (C) Immunofluorescence of FOXF1 demonstrating high expression in a subset of GATA6-positive cells (putative extraembryonic mesenchyme). (D) Expression of *FOXF1* in the inducible human embryoid single cell sequencing dataset. (E) Immunofluorescence of TBX20 demonstrating high expression in a subset of GATA6-positive cells (putative extraembryonic mesenchyme). (F) Expression of *TBX20* in the inducible human embryoid single cell sequencing dataset.

bioRxiv preprint doi: https://doi.org/10.1101/2023.06.15.545082; this version posted June 15, 2023. The copyright holder for this preprint (which was not certified by peer review) is the author/funder, who has granted bioRxiv a license to display the preprint in perpetuity. It is made available under aCC-BY-NC-ND 4.0 International license.

Extended Figure 7

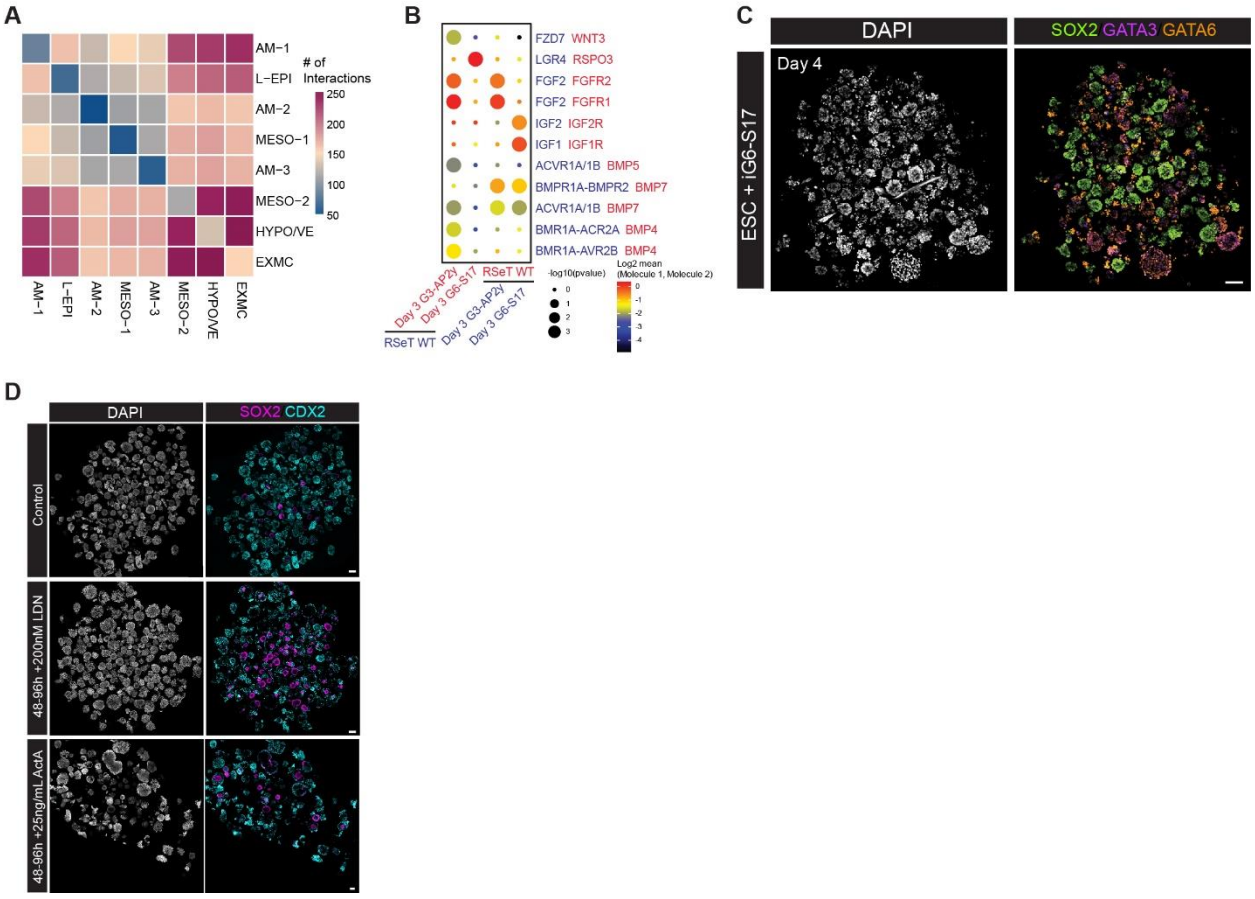

Extended Figure 7 (related to Fig 4) – Importance of BMP and inducible GATA3-AP2γ cells in generating inducible human embryoids.

(A) Predicted interaction map between clusters generated with CellPhoneDB. (B) Predicted interactions of inducible GATA6-SOX17 (G6-S17) and inducible GATA3-AP2γ (G3-AP2γ) cells after 3 days induction with wildtype RSeT hESCs, which are the cell types aggregated to generate inducible human embryoids. (C) Inducible human embryoids do not form if induced GATA3-AP2γ cells are excluded. (D) Overview of whole Aggrewells demonstrating the effect of BMP inhibition of NODAL activation. Note the significant increase in well-organized structures expressing SOX2 after BMP inhibition.

bioRxiv preprint doi: https://doi.org/10.1101/2023.06.15.545082; this version posted June 15, 2023. The copyright holder for this preprint (which was not certified by peer review) is the author/funder, who has granted bioRxiv a license to display the preprint in perpetuity. It is made available under aCC-BY-NC-ND 4.0 International license.

Extended Figure 8

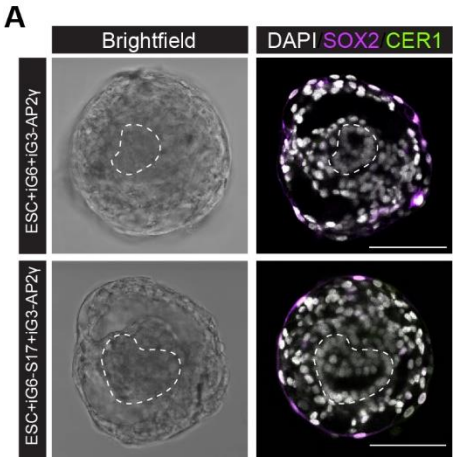

Extended Figure 8 (related to Fig 5) – CER1 expression is downregulated upon extend culture of inducible human embryoids

(A) Immunofluorescence of CER1 and SOX2 at day 6 post-aggregation demonstrates downregulation of both SOX2 and CER1 at this stage in structures generated with both inducible GATA6 (iG6) or inducible GATA6-SOX17 (iG6-S17) hypoblast-like cells together with wildtype ESCs and inducible GATA3-AP2γ (iG3-AP2γ cells.

bioRxiv preprint doi: https://doi.org/10.1101/2023.06.15.545082; this version posted June 15, 2023. The copyright holder for this preprint (which was not certified by peer review) is the author/funder, who has granted bioRxiv a license to display the preprint in perpetuity. It is made available under aCC-BY-NC-ND 4.0 International license.

Extended Table 1: Differentially Expressed Transcripts, Differentially Accessible Motifs, and Differentially Accessible Peaks between Cell Lines

Extended Table 2: Differentially Expressed Transcripts, Differentially Accessible Motifs, and Differentially Accessible Peaks between inducible Human Embryoid Course Cell Assignments